Nonlinear Mechanics of Thermoelastic Accretion

Fabio Sozio[1], Mostafa Faghih Shojaei[1], Souhayl Sadik[2,3], and Arash Yavari*[1,4]

[1] *School of Civil and Environmental Engineering, Georgia Institute of Technology, Atlanta, GA 30332, USA*
[2] *Max Planck Institute for Mathematics in the Sciences, D-04103 Leipzig, Germany*
[3] *Department of Engineering, Aarhus University, 8000 Aarhus C, Denmark*
[4] *The George W. Woodruff School of Mechanical Engineering, Georgia Institute of Technology, Atlanta, GA 30332, USA*

March 24, 2020

Abstract

In this paper, we formulate a theory for the coupling of accretion mechanics and thermoelasticity. We present an analytical formulation of the thermoelastic accretion of an infinite cylinder and of a two-dimensional block. We develop a numerical scheme for the solution of these two problems, and numerically calculate residual stresses and observe a strong dependence of the final mechanical state on the parameters of the accretion process. This suggests the possibility to predict and control thermal accretion processes of soft materials by manipulating thermal parameters, and therefore, to realize additively-manufactured soft objects with the desired characteristics and performances.

Keywords: Growth, accretion, thermoelasticity, nonlinear elasticity, residual stress, additive manufacturing.

1 Introduction

Accretion is the growth of a deformable solid by the gradual addition of material on its boundary. Unlike in bulk growth, where the material points are preserved, the set of material points in accretion problems is time dependent. We refer by thermal accretion to the class of processes and phenomena where thermal effects cannot be neglected in the characterization of the final accreted body, or where the growth process itself is driven by the temperature field through a change of phase. Additive manufacturing and solidification are important examples of thermal accretion. In order to formulate a thermoelastic accretion model, one needs to couple thermoelasticty and accretion mechanics.

Additive manufacturing, most commonly known as 3D printing, is unarguably a central part of what seems to be a revolutionary era in manufacturing and it is playing an ever increasing role in our everyday lives. It has already found many applications ranging from hobbyist art to precise manufacturing in various industries such as mechanical, aerospace, and medical [Gu et al., 2012; Horn and Harrysson, 2012; Huang et al., 2013]. Additive manufacturing was initially introduced in the 1980s for rapid prototyping. However, given its high efficiency, flexibility, and the mass customization possibilities, it was further developed for precise on-demand manufacturing and is now even considered a viable alternative to traditional manufacturing technologies [Levy et al., 2003; Frazier, 2010; Horn and Harrysson, 2012; Gu et al., 2012]. Additive manufacturing is further regarded as the pioneering production/manufacturing technology for "The Third Industrial Revolution" [Rifkin, 2011; Weller et al., 2015]. Despite its tremendous potential and commercial success, many challenges have yet to be overcome before additive manufacturing can be fully integrated in industry [Gu et al., 2012; Gibson et al., 2014; Frazier, 2014; Bikas et al., 2016]. From a mechanics point of view, understanding and being able to predict and control the residual stresses is crucial in order to tailor and design the process in such a way that the manufactured piece meets the required properties in its working conditions. As a matter of fact, the high temperatures and natural cooling that a piece undergoes during the additive manufacturing process causes large strains and can result in a high level of residual stresses [Shiomi et al., 2004; Mercelis and Kruth, 2006; Thompson et al., 2015; Shamsaei et al., 2015]. This may lead to severe part distortion, dimensional inaccuracies, and even

*Corresponding author, e-mail: arash.yavari@ce.gatech.edu

cracks in the final manufactured piece [Klingbeil et al., 2002; Dadbakhsh et al., 2012; Denlinger et al., 2015; Denlinger and Michaleris, 2017]. Such conditions put the additive manufacturing problem beyond the scope of the application of linearized elasticity. However, to the best of our knowledge, most of the existing works on additive manufacturing in the literature are based on linearized elasticity and/or are purely computational [Matsumoto et al., 2002; Ghosh and Choi, 2005; Zaeh and Branner, 2010; Michaleris, 2014; Li and Gu, 2014; Hodge et al., 2014; Loh et al., 2015; Hodge et al., 2016; Li et al., 2016; Bikas et al., 2016; Fergani et al., 2017; de La Batut et al., 2017].

The other main example of thermal accretion is the processes in which the material experiences a phase change (solidification) of the melt pool as it becomes part of the growing body. To this extent additive manufacturing technologies can be seen as a particular case of solidification, as new layers of material are deposited atop of old ones and fused together by melting the new material. In solidification problems, the growth surface is a phase change interface, on which a Stefan condition is imposed (see [Richmond and Tien, 1971; Viskanta, 1988; Stefan, 1989; Hu and Argyropoulos, 1996; Schwerdtfeger et al., 1998; Hodge et al., 2014] and references therein).

The formulation of the initial-boundary value problems of accretion processes and the mechanics of accretion at finite strains is still at its infancy. Additive manufacturing advances are good motivations for building a mathematical theory of the thermo-mechanics of accretion at finite strains that can be used in these new technologies. Compared to bulk growth (see [Epstein and Maugin, 2000; Garikipati et al., 2004; Yavari, 2010] and the book by Goriely [2017] summarizing the recent developments in bulk growth in biology), the mechanics of accretion is much less developed mainly because of the complexities involved in modeling the kinematics of accretion, especially for finite deformations, and the intrinsic incompatible nature of accreting bodies. Recently, Tomassetti et al. [2016] modeled a spherically-symmetric accretion of a hollow spherical ball made of an incompressible nonlinear elastic solid, coupling nonlinear elasticity, accretion and diffusion. A theory of diffusive accretion has recently been presented in [Abi-Akl et al., 2019]. Swain and Gupta [2018] formulated the thermodynamics of accretion by considering the diffusion of nutrients. In their formulation, the growth surface is treated as an interface whose motion is coupled with the other degrees of freedom. In another recent work on growth and accretion, Ganghoffer and Goda [2018] used configurational forces in the setting of irreversible thermodynamics. In [Truskinovsky and Zurlo, 2019] the accretion-induced incompatibilities are studied. In [Sozio and Yavari, 2017] a geometric theory of nonlinear accretion mechanics for symmetric surface growth of cylindrical and spherical bodies was introduced. This theory was used for the analysis of several model problems. Sozio and Yavari [2019a] formulated a geometric nonlinear theory of the mechanics of accretion without any symmetry assumptions. In this theory a body is represented by a time-dependent Riemannian manifold with a time-independent metric that at each point depends on the state of deformation at that point at its time of attachment to the body, and on the way the new material is added to the body. The accretion-induced incompatibilities were studied by calculating the curvature of the material metric, and the initial-boundary value problem of accretion was formulated. Some analytical results were provided for some special cases of accretion, and several nonlinear accretion problems were solved numerically. In this paper, the theory of [Sozio and Yavari, 2017, 2019a] will be extended to take into account the thermal effects. It should be emphasized that our focus in the present work is on the formulation of a geometric model that is able to take into account the attachment of new particles to a solid undergoing finite deformations (accretion) together with the heat conduction and thermal expansion effects; we do not consider phase transition phenomena or chemical reactions.

This paper is structured as follows. In §2 we formulate the coupling of nonlinear thermoelasticity with nonlinear accretion; we show how to build a material manifold taking into account thermal expansion/contraction together with the incompatibilities arising from the addition of new material and encoding everything into the material metric. In §3 we look at the radial thermo-accretion of an infinite cylinder under the assumption of axi-symmetry. This is a one-dimensional problem that we solve using the finite difference method. In §4 we consider the vertical growth of a two-dimensional block and solve it using an efficient discretization of a weak formulation of the problem. Conclusions, some final comments, and a brief discussion of future work are given in §5.

2 Coupling of Thermoelasticity and Accretion

In this section we review some elements of nonlinear thermoelasticity and accretion mechanics. For more details on geometric nonlinear elasticity see [Marsden and Hughes, 1983], on thermoelasticity [Ozakin and Yavari, 2010; Sadik and Yavari, 2017], and on nonlinear accretion mechanics [Sozio and Yavari, 2017, 2019a]. Let $\mathcal{S}$ be the three-dimensional Euclidean ambient space, and $\boldsymbol{g}$ its usual scalar product. We indicate with $\mathcal{B}_t$ the configuration representing the accreting body at time t. Once $\mathcal{B}_t$ is defined, our goal is to endow it with an *a priori* unknown inner product $\boldsymbol{G}$ representing its fully relaxed state. Note that this state may not be realizable in the physical three-dimensional Euclidean space, whence the presence of residual stresses. We denote by $\{X^A\}$ and $\{x^a\}$ the local coordinates on $\mathcal{B}_t$ and $\mathcal{S}$, respectively. $\nabla^{\boldsymbol{G}}$ and $\nabla^{\boldsymbol{g}}$ are the Levi-Civita connections of $(\mathcal{B}_t, \boldsymbol{G})$ and $(\mathcal{S}, \boldsymbol{g})$, repectively. We denote their respective Christoffel symbols by $\Gamma^A{}_{BC}$, and $\gamma^a{}_{bc}$ in the local coordinate charts $\{X^A\}$ and $\{x^a\}$, respectively. We also adopt Einstein's repeated index summation convention.

2.1 Kinematics of accretion

During an accretion process, the material manifold representing a growing body is not fixed in time. Indeed, new material points are attached to the part of the boundary of the body called the growth surface. The growing body is identified with a time-dependent three-dimensional manifold $\mathcal{B}_t$. We assume that $t = 0$ corresponds to the start of the growth process and t_f to the end. In light of this discussion, an accreting body is modeled as a connected $\mathcal{S}$-embeddable 3-manifold $\mathcal{M}$ together with a smooth map $\tau : \mathcal{M} \to [0, t_f]$, called the time of attachment map [Sozio and Yavari, 2019a]. The body at time t is represented by the set

$$\mathcal{B}_t = \{X \in \mathcal{M} \mid \tau(X) \leq t\},$$

while the level surface $\Omega_t = \tau^{-1}(t)$ is the aforementioned growth surface at time t. The motion of a body subject to accretion is a time-dependent map with a time-dependent domain, i.e., a family of maps $\varphi_t : \mathcal{B}_t \to \mathcal{S}$, with $t \in [0, t_f]$. The so-called deformation gradient $\boldsymbol{F}_t$ is the derivative map of φ_t defined as $\boldsymbol{F}_t(X) = T\varphi_t(X)$ and is a two-point tensor $\boldsymbol{F}_t(X) : T_X\mathcal{B} \to T_{\varphi_t(X)}\mathcal{S}$. The frozen deformation gradient is a two-point tensor $\bar{\boldsymbol{F}}$ defined as $\bar{\boldsymbol{F}}(X) = \boldsymbol{F}_{\tau(X)}(X)$, recording the deformation gradient of each point X at its time of attachment $\tau(X)$. Note that, in general, $\bar{\boldsymbol{F}}$ is not the tangent map of a deformation, i.e., it is not a deformation gradient. We indicate with $\boldsymbol{U}$ the velocity of the material motion describing the evolution of the layers Ω_t in time, representing the growth velocity in the material manifold. Note however that the material motion is not unique; it can be shown that there is some freedom in its choice within a class of material motions that leave the accretion initial-boundary value problem unaltered [Sozio and Yavari, 2019a]. We denote the growth surface in the deformed configuration by $\omega_t = \varphi_t(\Omega_t)$, i.e., the part of the deformed boundary where material points are added. The total velocity of the growth surface ω in the deformed configuration has two contributions: one due to accretion, and one due to deformation. Its velocity $\boldsymbol{w}$ is called the total velocity, and can be written as $\boldsymbol{w} = \bar{\boldsymbol{F}}\boldsymbol{U} + \boldsymbol{v}$. The term $\bar{\boldsymbol{F}}\boldsymbol{U}$ represents the contribution of accretion, while $\boldsymbol{v}$ is the standard velocity of points as material particles moving in the ambient space via φ_t.

We assume that at time t one can univocally identify a vector field $\boldsymbol{u}_t$ on ω_t called the growth velocity that describes the rate and direction at which new material is being added. Alternatively, for every material point X, we define a time-independent growth "velocity" $\boldsymbol{u} : \mathcal{B} \to T\mathcal{S}$ by assigning to each point X the growth velocity at its time of attachement to the body, i.e., $\boldsymbol{u} := \boldsymbol{u}_{\tau(X)} \circ \varphi_{\tau(X)}$. Contrary to our intuition, $\bar{\boldsymbol{F}}\boldsymbol{U}$ and $\boldsymbol{u}$ are two different objects, although there are some cases (such as traction-free growth surface) in which they coincide [Sozio and Yavari, 2019a]. Note that the growth velocity $\boldsymbol{u}$ can be seen as a parameter of the additive manufacturing process. Note also that we have assumed that the growth velocity is a given vector field on the boundary of the deformed body. However, in a coupled theory of accretion it would be one of the unknown fields.

2.2 The material metric

A material metric $\boldsymbol{G}$ is constructed to give at every time t an abstract material Riemannian manifold $(\mathcal{B}_t, \boldsymbol{G})$, where the distances measured by $\boldsymbol{G}$ correspond to a fully relaxed state. Note that this state may not be realizable in the physical three-dimensional Euclidean space but it is indeed realizable as an abstract Riemannian manifold. The material metric explicitly depends on the history of loading during the surface growth process as well as

the temperature field $T = T(X,t)$ and the thermal expansion proprieties of the solid. In thermoelasticity, one may write the material metric as [Ozakin and Yavari, 2010; Sadik and Yavari, 2017][1]

$$\boldsymbol{G}(X,T) = e^{\boldsymbol{\omega}^\star(X,T)}\boldsymbol{G}_0(X)e^{\boldsymbol{\omega}(X,T)}\,. \tag{1}$$

Here, $\boldsymbol{\omega} = \boldsymbol{\omega}(X,T)$ is a $\binom{1}{1}$-rank temperature-dependent tensor characterizing the thermal extension properties of the solid. It depends on the thermal expansion characteristics of the material and is such that $\boldsymbol{\omega}(X,T_0(X)) = \boldsymbol{0}$, where $T_0(X)$ is a reference temperature field. Therefore, one has $\boldsymbol{G}_0 = \boldsymbol{G}(X,T_0)$. In components, (1) reads $G_{AB} = e^{\omega^C{}_A}\,(G_0)_{CD}\,e^{\omega^D{}_B}$. In the particular case of isotropic thermal expansion, the material metric reduces to

$$\boldsymbol{G}(X,T) = e^{2\omega(X,T)}\boldsymbol{G}_0(X)\,,$$

where $\omega = \omega(X,T)$ is a scalar, with $\omega(X,T_0(X)) = 0$. The coefficient of thermal expansion reads $\alpha(X,T) = \partial\omega(X,T)/\partial T$, so one has

$$\omega(T) = \int_{T_0}^{T}\alpha(\eta)\mathrm{d}\eta\,. \tag{2}$$

In thermal accretion, we choose the field $T_0 = T_0(X)$ as the temperature at which the new material is added so that $\boldsymbol{G}_0$ is a temperature-independent metric that depends only on the history of loading during the accretion process. Note that when the material metric is written in the form (1), the thermoelasticity effects are fully encoded in $\boldsymbol{\omega}$ while the accretion and history of loading during growth are fully encoded in $\boldsymbol{G}_0$.

In order to calculate $\boldsymbol{G}_0$, we define the accretion tensor $\boldsymbol{Q}$ as the time-independent two-point tensor field given by [Sozio and Yavari, 2019a]

$$\boldsymbol{Q} = \bar{\boldsymbol{F}} + (\boldsymbol{u} - \bar{\boldsymbol{F}}\boldsymbol{U})\otimes\mathrm{d}\tau\,,$$

which agrees with the frozen deformation gradient $\bar{\boldsymbol{F}}$ on each layer, and is such that $\boldsymbol{Q}\boldsymbol{U} = \boldsymbol{u}$. The accretion tensor can be understood as the gradient of a mapping that takes a layer of material in the material manifold and maps it to its current configuration right before attachment. For this reason, we define the material metric on $\mathcal{B}_t$ as the pull-back of the Euclidean ambient metric $\boldsymbol{g}$ through $\boldsymbol{Q}$, i.e., as

$$\boldsymbol{G}_0(X) = \boldsymbol{Q}^\star(X)\,\boldsymbol{g}(\varphi(X,\tau(X)))\,\boldsymbol{Q}(X)\,. \tag{3}$$

In components, one has $(G_0)_{IJ} = Q^i{}_I\,g_{ij}\,Q^j{}_J$. Plugging (1) into (3), one then obtains

$$\boldsymbol{G}(X,T) = e^{\boldsymbol{\omega}^\star(X,T)}\boldsymbol{Q}^\star(X)\,\boldsymbol{g}(\varphi(X,\tau(X)))\,\boldsymbol{Q}(X)\,e^{\boldsymbol{\omega}(X,T)}\,. \tag{4}$$

When the growth surface is traction-free, one can show that if the energy function is rank-1 convex, then $\boldsymbol{Q} = \bar{\boldsymbol{F}}$ [Sozio and Yavari, 2019a].[2] Note that in this case $\bar{\boldsymbol{F}}\boldsymbol{U} = \boldsymbol{u}$, as $\boldsymbol{Q}\boldsymbol{U} = \boldsymbol{u}$ by construction.

By virtue of (1), the Riemannian volume form for $\boldsymbol{G}$ in the isotropic case reads $\mathrm{d}V = e^{\operatorname{tr}\boldsymbol{\omega}}\mathrm{d}V_0$, where $\mathrm{d}V_0$ is the Riemannian volume form for $\boldsymbol{G}_0$. The Jacobian J relates the material and spatial Riemannian volume elements $\mathrm{d}V$ and $\mathrm{d}v$ as $\mathrm{d}v = J\mathrm{d}V$. It can be shown that

$$J = \sqrt{\frac{\det\boldsymbol{g}}{\det\boldsymbol{G}}}\det\boldsymbol{F} = \frac{\det\boldsymbol{F}}{\det\boldsymbol{Q}}e^{-\operatorname{tr}\boldsymbol{\omega}}\,, \tag{5}$$

where use was made of (4). Note that in the isotropic case one has $e^{\operatorname{tr}\boldsymbol{\omega}(X,T)} = e^{3\omega(X,T)}$, or $e^{\operatorname{tr}\boldsymbol{\omega}(X,T)} = e^{2\omega(X,T)}$ in 2D problems.

In the setting of nonlinear mechanics, incompatibility is quantified by either the curl of the accretion tensor $\boldsymbol{Q}$, or by the curvature of the material metric $\boldsymbol{G}$. This is studied in [Sozio and Yavari, 2019a] when thermal effects are ignored. In the present paper we do not focus on the study of incompatibility, which is implicitly encoded in the tensor $\boldsymbol{Q}$ (or in some cases $\bar{\boldsymbol{F}}$).

[1] We denote by $\boldsymbol{T}^\star$ the dual of the $\binom{1}{1}$-rank tensor $\boldsymbol{T}$: operating on a 1-form $\boldsymbol{\lambda}$, it contracts its upper index with $\boldsymbol{\lambda}$, i.e., $\boldsymbol{T}^\star\boldsymbol{\lambda} = T^B{}_A\lambda_B\mathrm{d}X^A$. It should not be confused with the adjoint operator $^\mathsf{T}$, cf. footnote 3.

[2] Rank-1 convexity allowed Sozio and Yavari [2019a] to use an energetic argument to show that the absence of in-layer deformation and the vanishing of out-of-layer stress (tractions) imply $\bar{\boldsymbol{F}} = \boldsymbol{Q}$. Note that being an isometry, the accretion tensor $\boldsymbol{Q}$ represents an undeformed state.

2.3 Balance of mass

Let ρ and ϱ respectively denote the material and spatial mass densities. Although mass conservation does not hold globally for a body undergoing accretion, mass is locally conserved in the body away from the growth surface. For any open set $\mathcal{U}$ in $\mathcal{B}_t$, conservation of mass is written as

$$\int_{\varphi_t(\mathcal{U})} \varrho \, \mathrm{d}v = \int_{\mathcal{U}} \rho \, \mathrm{d}V = \int_{\mathcal{U}} \rho_0 \, \mathrm{d}V_0 \,,$$

where $\rho_0(X)$ is the material mass density at $T = T_0(X)$—the temperature field corresponding to the stress-free metric $\boldsymbol{G}_0$. Localizing the above equation gives the local form of mass conservation

$$\rho(X,t) = J(X,t)\varrho(X,t) \,,$$

where the material mass density ρ is related to the reference material mass density ρ_0 via

$$\rho_0(X) = e^{\operatorname{tr} \boldsymbol{\omega}(X,T(X,t))}\rho(X,t) \,, \tag{6}$$

so that $\rho_0 = Je^{\operatorname{tr}\boldsymbol{\omega}}\varrho$.

2.4 Stress tensors and the balance of linear momentum

The right Cauchy-Green deformation tensor is defined as $\boldsymbol{C} = \boldsymbol{F}^{\mathsf{T}}\boldsymbol{F}$;[3] in components, $C^A{}_B = G^{AK}F^a{}_K g_{ab}F^b{}_B$. Note that $\boldsymbol{C}^\flat$ is the pull-back of the spatial metric $\boldsymbol{g}$ by φ, i.e., $\boldsymbol{C}^\flat = \varphi^*\boldsymbol{g}$, where $^\flat$ denotes the flat operator for lowering tensor indices. The left Cauchy-Green deformation tensor (also called Finger tensor) is defined as $\boldsymbol{b} = \boldsymbol{F}\boldsymbol{F}^{\mathsf{T}}$; in components, $b^a{}_b = F^a{}_A F^c{}_B G^{AB} g_{cb}$. Note that $\boldsymbol{b}^\sharp$ agrees with the push-forward of the inverse material metric $\boldsymbol{G}^\sharp$ by φ, i.e., $\boldsymbol{b}^\sharp = \varphi_*\boldsymbol{G}^\sharp$, where $^\sharp$ denotes the sharp operator that is used for raising tensor indices.

We assume that the body is made of a hyperelastic material, so that the constitutive model is given by an energy function $\mathcal{W} = \tilde{\mathcal{W}}(X, T, \boldsymbol{F}, \boldsymbol{g}, \boldsymbol{G})$ per unit undeformed volume, and the Cauchy and the first Piola-Kirchhoff stress tensors are defined as

$$\boldsymbol{\sigma} = \frac{2}{J}\frac{\partial \tilde{\mathcal{W}}}{\partial \boldsymbol{g}} \,, \qquad \boldsymbol{P} = \frac{\partial \tilde{\mathcal{W}}}{\partial \boldsymbol{F}} \,,$$

where $J\boldsymbol{\sigma} = \boldsymbol{P}\boldsymbol{F}^\star$. If the material is incompressible, we have $J = 1$ and the Cauchy stress tensor is written as

$$\boldsymbol{\sigma} = 2\frac{\partial \tilde{\mathcal{W}}}{\partial \boldsymbol{g}} - p\,\boldsymbol{g}^\sharp \,, \qquad \boldsymbol{P} = \frac{\partial \tilde{\mathcal{W}}}{\partial \boldsymbol{F}} - p\,\boldsymbol{g}^\sharp \boldsymbol{F}^{-\star} \,,$$

where p is the Lagrange multiplier associated with the incompressibility constraint. For neo-Hookean incompressible materials the energy density is written as

$$\tilde{\mathcal{W}}(X, T, \boldsymbol{F}, \boldsymbol{g}, \boldsymbol{G}) = \frac{\mu(T)}{2}\operatorname{tr}\boldsymbol{C} - p(J-1)^2 \,,$$

where $\boldsymbol{C}$ and J depend on the temperature through the material metric $\boldsymbol{G}$ (see Appendix A). The Cauchy and the first Piola-Kirchhoff stress tensors are expressed as

$$\boldsymbol{\sigma} = \mu\boldsymbol{b}^\sharp - p\boldsymbol{g}^\sharp \,, \qquad \boldsymbol{P} = \mu\boldsymbol{F}\boldsymbol{G}^\sharp - p\boldsymbol{g}^\sharp\boldsymbol{F}^{-\star} \,. \tag{7}$$

We consider slow accretion processes. Ignoring the inertial term, the balance of linear momentum reads

$$\operatorname{div}\boldsymbol{\sigma} + \varrho\mathbf{f} = \mathbf{0} \,, \qquad \operatorname{Div}\boldsymbol{P} + \rho\mathbf{f} = \mathbf{0} \,, \tag{8}$$

where div denotes the spatial divergence operator with respect to the metric $\boldsymbol{g}$, Div the material divergence operator with respect to the metrics $\boldsymbol{g}$ and $\boldsymbol{G}$, and $\mathbf{f}$ denotes the body force per unit mass.

[3] We denote the adjoint of $\boldsymbol{F}$ by $\boldsymbol{F}^{\mathsf{T}}$ and it is defined such that $\boldsymbol{g}(\boldsymbol{F}\boldsymbol{W}, \boldsymbol{w}) = \boldsymbol{G}(\boldsymbol{W}, \boldsymbol{F}^{\mathsf{T}}\boldsymbol{w})$ for any pair $(\boldsymbol{W}, \boldsymbol{w}) \in T_X\mathcal{B}_t \times T_{\varphi_t(X)}\mathcal{S}$. In components, $(F^{\mathsf{T}})^A{}_a = g_{ab}F^b{}_B G^{AB}$.

2.5 The heat equation

Starting from the fundamental laws of thermodynamics, one can find the following generalized heat equation [Dillon Jr, 1962; Sadik and Yavari, 2017]

$$\operatorname{Div} \boldsymbol{H} = -\rho c_E \dot{T} + \frac{1}{2} T \frac{\partial \boldsymbol{S}}{\partial T} : \dot{\boldsymbol{C}}^{\flat} + \rho R \,, \tag{9}$$

where $\boldsymbol{H}$ is the material heat flux vector per unit area, c_E denotes the specific heat capacity at constant strain, and R is the external specific heat supply. For a thermally isotropic solid, the heat flux response function has the following representation [Truesdell and Noll, 2004, p. 358]

$$\boldsymbol{H} = (\phi_0 \boldsymbol{C}^{-\sharp} + \phi_1 \boldsymbol{G}^{\sharp} + \phi_2 \boldsymbol{C}^{\sharp}) \mathrm{d}T \,,$$

where $\mathrm{d}T = \frac{\partial T}{\partial X^A} dX^A$, and $\phi_k = \phi_k(X, T, \mathrm{d}T, \boldsymbol{C}, \boldsymbol{G})$, $k = -1, 0, 1$, are scalar functions. If we set $\boldsymbol{K} = -(\phi_0 \boldsymbol{C}^{-\sharp} + \phi_1 \boldsymbol{G}^{\sharp} + \phi_2 \boldsymbol{C}^{\sharp})$, then by the reduced form of the Clausius-Duhem inequality $\langle \mathrm{d}T, \boldsymbol{H} \rangle \leq 0$,[4] and hence, $\boldsymbol{K}$ is a positive semi-definite symmetric material $\binom{2}{0}$-tensor (the heat conductivity tensor). One can write a generalized version of the Fourier's law of thermal conduction as $\boldsymbol{H} = -\boldsymbol{K}\mathrm{d}T$. In our numerical examples we consider the simple model $\boldsymbol{K} = K\boldsymbol{G}^{\sharp}$, where K is the heat conduction coefficient, while we call $D = \frac{K}{c_E \rho}$ the diffusivity coefficient. Therefore, the heat equation (9) is simplified to read[5]

$$\operatorname{Div}\left(K \boldsymbol{G}^{\sharp} \mathrm{d}T\right) = \rho c_E \dot{T} - \frac{1}{2} T \frac{\partial \boldsymbol{S}}{\partial T} : \dot{\boldsymbol{C}}^{\flat} - \rho R \,. \tag{10}$$

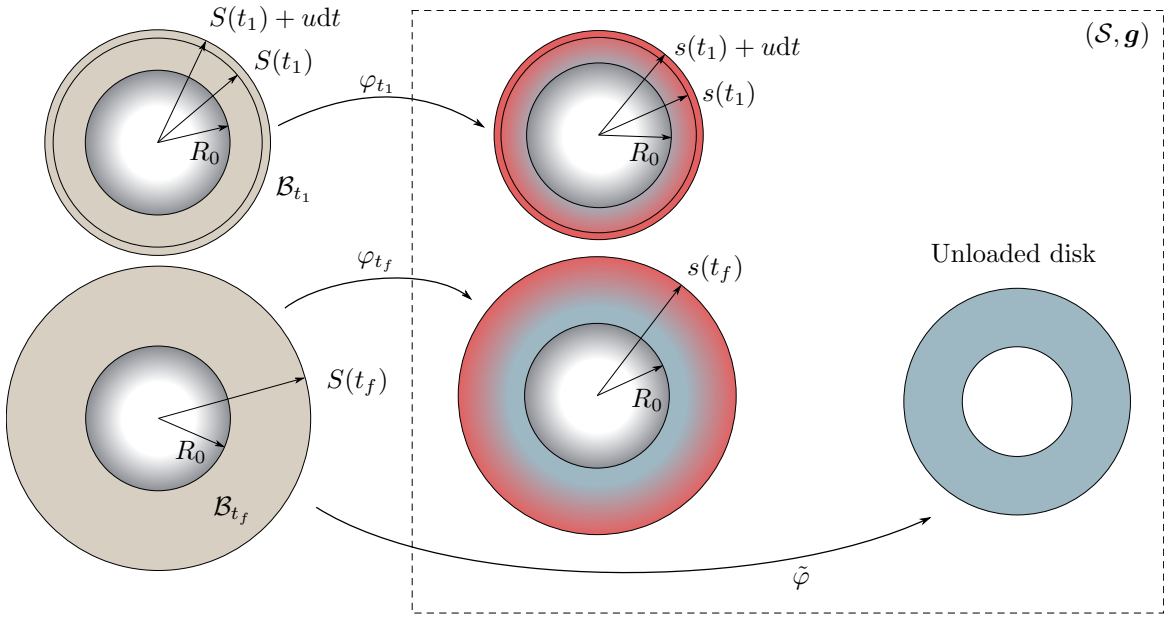

Figure 1: *Configurations of a radially-symmetric accreting hollow cylinder on a rigid substrate (inner disk in gray). Top two disks: Material and deformed configurations at time t_1, $0 < t_1 < t_f$. Bottom left two disks: Material and deformed configurations at the final time t_f. Bottom right disk: When accretion is completed one unloads and lets the cylinder cool down. The result is a residually-stressed configuration.*

3 Accretion of a hollow cylinder

In this section, we present a simplified formulation of the thermoelastic problem for the radially-symmetric accretion of an infinitely-long hollow cylinder (see Fig. 1). We assume that the material is initially added on

[4] In Appendix D we discuss the derivation of this inequality.
[5] Note that $\boldsymbol{G}^{\sharp}\mathrm{d}T = \operatorname{Grad} T$.

the outer surface of a rigid and infinitely-long cylindrical substrate of radius R_0 and that the growing cylinder is sitting in an ambient temperature T_a. We assume that stress-free cylindrical layers of new material are continuously and uniformly formed on the outer boundary of the cylinder at a temperature T_m—its melting temperature—greater than T_a. The growth velocity is assumed to be normal to the growth surface and has magnitude $u(t)$. The added rings are made of the same homogeneous isotropic incompressible material, with a uniform isotropic coefficient of thermal expansion $\alpha(T)$, and a uniform isotropic coefficient of heat conduction $K(T)$. Assuming an infinitely-long cylinder, the problem is reduced to studying a cross section of the cylinder, i.e., the surface growth of a two-dimensional annulus. Let (R, Θ) and (r, θ) be the polar coordinates in the material manifold $\mathcal{B}_t$—which has yet to be constructed—and the ambient space $\mathcal{S}$, respectively. The ambient space metric $\boldsymbol{g}$ is represented in polar coordinates by a diagonal matrix $\mathrm{diag}(1, r^2)$.

3.1 The material manifold

The first task is to construct a time-dependent material manifold $\mathcal{B}_t$ resulting from the addition of the new rings. We denote by $S(t)$ the material external radius of the growing cylinder, so that

$$\mathcal{B}_t = \{(R, \Theta) : R_0 < R \leq S(t)\,, 0 \leq \Theta < 2\pi\}\,.$$

Note that since we are concerned with a model for continuous accretion with no ablation, $S(t)$ is assumed to be a continuous bijective mapping. One can hence define its inverse map $\tau = S^{-1}$ assigning to each ring at $R \geq R_0$ its time of attachment $\tau(R)$ as defined in §2.1. Assuming that accretion starts at $t = 0$, it follows that $\tau(R_0) = 0$ and equivalently that $S(0) = R_0$. We define the material growth velocity $U(t) = \dot{S}(t)$, which yields $S(t) = R_0 + \int_0^t U(\nu)\mathrm{d}\nu$. In what follows, we choose $S(t)$ such that $U(t) = u(t)$,[6] which means that in the time interval $[t, t + \mathrm{d}t]$ the external radii of both the material and spatial disks grow by the amount $u(t)\mathrm{d}t$ (see Fig. 1). Hence, $S(t) = R_0 + \int_0^t u(\nu)\mathrm{d}\nu$.

Kinematics of the accreting cylinder. We assume that the growing cylinder deforms in a radially-symmetric fashion, i.e., we take motions φ_t of the kind $(r(R, t), \Theta)$. The deformation gradient reads

$$\boldsymbol{F}(R, t) = \begin{bmatrix} r_{,R}(R, t) & 0 \\ 0 & 1 \end{bmatrix}\,, \tag{11}$$

where a subscript comma denotes partial differentiation, e.g., $r_{,R}(R, t) = \frac{\partial r}{\partial R}(R, t)$. As was mentioned earlier, as the growth surface $R = S(t)$ is traction-free, $\boldsymbol{Q} = \bar{\boldsymbol{F}}$, and hence, $\boldsymbol{u} = \bar{\boldsymbol{F}}\boldsymbol{U}$. Therefore, the material growth speed U and the spatial growth speed u are related as

$$u(t) = r_{,R}(S(t), t)\, U(t)\,. \tag{12}$$

This is equivalent to assuming the absence of traction on the outer boundary, see [Sozio and Yavari, 2019a]. Having already assumed $U(t) = u(t)$, Eq. (12) gives us

$$r_{,R}(S(t), t) = 1\,, \quad \text{or} \quad r_{,R}(R, \tau(R)) = 1\,, \tag{13}$$

so that the frozen deformation gradient reads $\bar{\boldsymbol{F}} = \boldsymbol{I}$, see §2.1. We introduce the notation $s(t) = r(S(t), t)$, see Fig. 1, and $\bar{r}(R) = r(R, \tau(R))$, so that one has $s = \bar{r} \circ S$ or $\bar{r} = s \circ \tau$. Finally, the rate of change of the spatial radius of the growing cylinder $s(t) = r(S(t), t)$, representing the radial and the only non-zero component of the total velocity $\boldsymbol{w}$, is written as

$$\dot{s}(t) = \frac{\mathrm{d}}{\mathrm{d}t}[r(S(t), t)] = r_{,R}(S(t), t)\dot{S}(t) + r_{,t}(S(t), t) = \dot{S}(t) + r_{,t}(S(t), t)\,, \tag{14}$$

where $r_{,t} = \partial r/\partial t$ is the radial and only non-zero component of the standard velocity $\boldsymbol{v}$. From (14), it follows that the velocity of the accretion boundary is the result of two contributions: $\dot{S}(t) = U(t) = u(t)$, due merely to accretion, and the standard velocity $r_{,t}(S(t), t)$.

[6] Note that there are many other choices that will result in the same stress calculation. As a matter of fact, for isotropic solids the geometric theory suggests that the material body is represented by a class of infinitely many isomorphic Riemannian manifolds. The anisotropic case is slightly more complicated as one needs to look at the symmetry group for the constitutive equation, but there is still some arbitrariness. This was discussed in detail in [Sozio and Yavari, 2017] and [Sozio and Yavari, 2019b].

3.2 The material metric

As was discussed earlier, given a material manifold $\mathcal{B}_t$, first one constructs a metric $\boldsymbol{G}_0$ for $\mathcal{B}_t$ taking into account the history of loading during the accretion process. Next, given the actual evolution of the temperature field T in the growing body, the material metric can be constructed following (1) and (2) as $\boldsymbol{G} = e^{2\omega(T)}\boldsymbol{G}_0$. Hence, following Sozio and Yavari [2017], a material metric for a ring of the material annulus $\mathcal{B}_t$ under the uniform temperature T_m is given by the pull-back of $\boldsymbol{g}$ by φ at its time of attachment $\tau(R)$ as in (3). Therefore, as we showed $\boldsymbol{Q}(R) = \bar{\boldsymbol{F}}(R) \equiv \boldsymbol{I}$, and hence one obtains

$$\boldsymbol{G}_0(R) = \begin{bmatrix} 1 & 0 \\ 0 & \bar{r}^2(R) \end{bmatrix} . \tag{15}$$

Note that the reference temperature field is $T_0 = T_m$. Then, by virtue of (4) and (15), the material metric reads

$$\boldsymbol{G}(R,t) = e^{2\omega(T(R,t))} \begin{bmatrix} 1 & 0 \\ 0 & \bar{r}^2(R) \end{bmatrix} , \tag{16}$$

where the function $\omega(T)$ is discussed in Appendix A.

3.3 Governing equations

From (11) and (16), the incompressibility condition $J = 1$ is written as

$$r(R,t)\, r_{,R}(R,t) = e^{2\omega(T)} \bar{r}(R,t) . \tag{17}$$

Thus, it follows that

$$r^2(R,t) = \int_{R_0}^{R} 2\bar{r}(\xi) e^{2\omega(T(\xi,t))} \mathrm{d}\xi + {R_0}^2 . \tag{18}$$

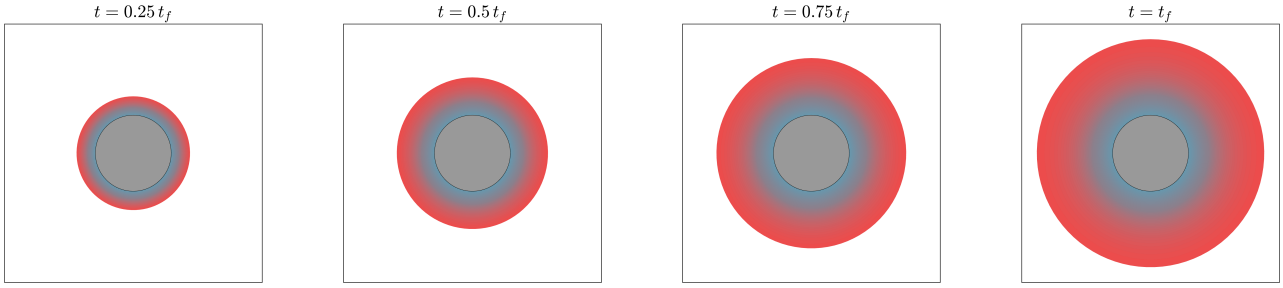

Figure 2: *The accreting cylinder at four different times $\frac{1}{4}t_f$, $\frac{1}{2}t_f$, $\frac{3}{4}t_f$, t_f. The lighter colors indicate higher temperatures. Note that the gray circle at the center representing the rigid internal substrate for the growing cylinder is identical in all the four figures; if the reader sees a difference, it is due to the Delboeuf illusion.*

As for the balance of linear momentum, we first compute the Finger deformation tensor, viz.

$$\boldsymbol{b}^\sharp = \begin{bmatrix} \frac{\bar{r}^2 e^{2\omega}}{r^2} & 0 \\ 0 & \frac{1}{\bar{r}^2 e^{2\omega}} \end{bmatrix} .$$

Therefore, following (7), the Cauchy stress tensor reads

$$\boldsymbol{\sigma} = \begin{bmatrix} \frac{\mu \bar{r}^2 e^{2\omega}}{r^2} - p & 0 \\ 0 & \frac{\mu}{\bar{r}^2 e^{2\omega}} - \frac{p}{r^2} \end{bmatrix} , \tag{19}$$

where p is the pressure field associated with the incompressibility condition, and the shear modulus μ depends on the temperature field and therefore on the radial coordinate and time, i.e., $\mu = \mu(T(R,t))$. The radial component of the equilibrium equation (8) is simplified to read

$$\sigma^{rr}{}_{,R} + \frac{r_{,R}}{r} \left(\sigma^{rr} - r^2 \sigma^{\theta\theta} \right) = 0 ,$$

Parameter	Symbol	Value
Internal material radius	R_0	1 L_o
Shear modulus	μ	1 μ_o
Accretion time	t_f	1 t_o
Melting temperature	T_m	1 T_o
Substrate temperature	T_s	0 T_o
Thermal expansion coefficient at T_a	α_a	0.25 T_o^{-1}
Heat transfer coefficient	h_s	2 $\frac{\mu_o L_o}{t_o T_o}$
Diffusivity coefficient	D	1 $\frac{L_o^2}{t_o}$

Table 1: *Parameters for the numerical calculations of the accreting cylinder.*

from which, by (19), it follows that

$$\sigma^{rr}{}_{,R} = \frac{\mu}{\bar{r}}\left(1 - \frac{\bar{r}^4 e^{4\omega}}{r^4}\right).$$

Since $\sigma^{rr}(S(t),t) = 0$, one obtains the following expression for the radial stress:

$$\sigma^{rr}(R,t) = -\int_R^{S(t)} \frac{\mu(T(\xi,t))}{\bar{r}(\xi)}\left[1 - \frac{\bar{r}^4(\xi)e^{4\omega(T(\xi,t))}}{r^4(\xi,t)}\right]\mathrm{d}\xi\,. \tag{20}$$

On the other hand, it follows from (19) that

$$\sigma^{\theta\theta} = \frac{\sigma^{rr}}{r^2} + \frac{\mu}{r^2}\left[\frac{r^2}{\bar{r}^2 e^{2\omega}} - \frac{\bar{r}^2 e^{2\omega}}{r^2}\right],$$

where r is given by (18).[7] Note that at $R = S(t)$, one has $\bar{r} = r$, and $T = T_m$—whence $\omega = 0$. Therefore, the stress-free boundary condition for the hoop stress, i.e., $\sigma^{\theta\theta}(S(t),t) = 0$, is trivially satisfied.[8] Once accretion is completed, one can calculate the residually stressed configuration $\tilde{r}(R)$ through (18) and (20) by imposing uniform $T = T_a$ and traction-free boundary conditions. The residual stresses are denoted by $\tilde{\sigma}^{rr}$ and $\tilde{\sigma}^{\theta\theta}$ (see Fig. 4).

Assuming that there is no external heat supply and neglecting the coupling term, the heat equation (10) simplifies to read

$$\mathrm{Div}\left(K\boldsymbol{G}^{\sharp}\mathrm{d}T\right) = \rho c_E \dot{T}\,. \tag{21}$$

Recalling from (6) that $\rho(R,t) = \rho_0(R)e^{-2\omega(T(R,t))}$, and from Appendix C, Eq. (21) is simplified to read

$$\frac{K}{\bar{r}}\left(\bar{r}(R)\frac{\partial T}{\partial R}\right)_{,R} + \frac{\mathrm{d}K}{\mathrm{d}T}T_{,R}{}^2 = \rho_0 c_E \dot{T}\,. \tag{22}$$

We assume a Neumann boundary condition on the inner boundary $R = R_0$:

$$\left[K(T)T_{,R} - h_a(T - T_a)\right]_{(R_0,t)} = 0\,, \tag{23}$$

where h_a is the heat transfer coefficient between the cylinder and the ambient air inside the hollow cylinder. On the growth surface $R = S(t)$, the temperature boundary condition is $T = T_m$.

[7] If the inner boundary is subject to a traction (pressure) p_i, the condition $\sigma^{rr}(S(t),t) = -p_i(t)$ gives the following equation

$$\int_{R_i}^{S(t)} \frac{\mu(T(\xi,t))}{\bar{r}(\xi)}\left[1 - \frac{\bar{r}^4(\xi)e^{4\omega(T(\xi,t))}}{r^4(\xi,t)}\right]\mathrm{d}\xi = p_i(t)\,.$$

[8] Note that $\sigma^{\theta\theta}(S(t),t) = 0$ is not assumed; it is anticipated by virtue of $\boldsymbol{Q} = \bar{\boldsymbol{F}}$.

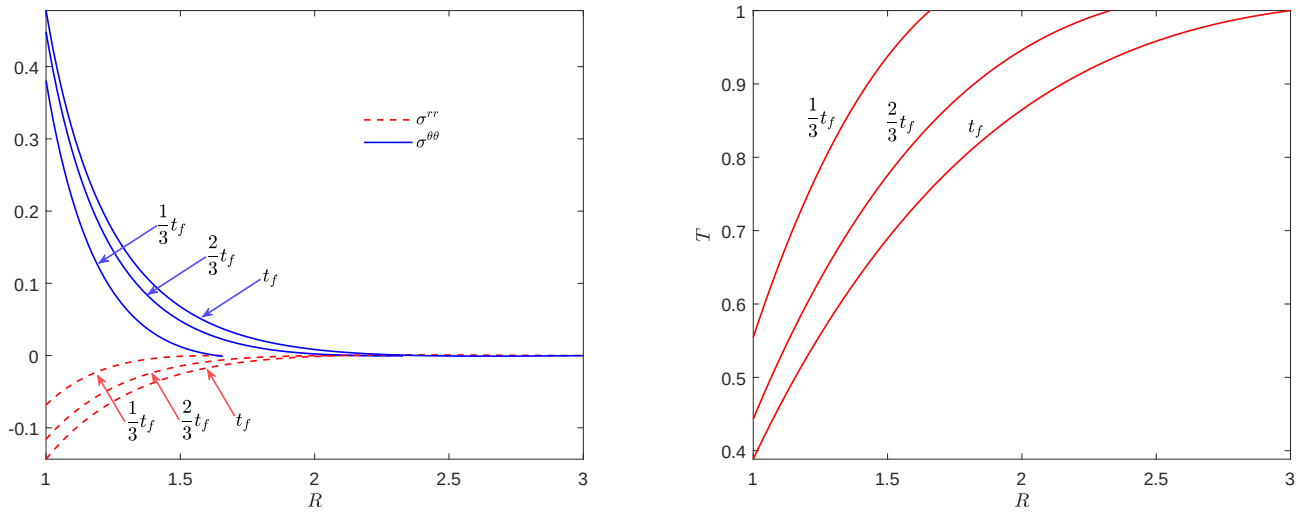

Figure 3: *Left: Radial and circumferential stresses σ^{rr} (red) and $\sigma^{\theta\theta}$ (blue) at three different times $\frac{1}{3}t_f$, $\frac{2}{3}t_f$, t_f. Note that $\sigma^{\theta\theta}$ has the dimension of a stress over an area, i.e., it is not a physical component. Its physical representation is $r^2\sigma^{\theta\theta}$, which is very close to $\sigma^{\theta\theta}$ as its highest value is at $R = 1$. Notice that both components of stress vanish at the outer surface, i.e., for $R = S(t)$, for any t. Right: Temperature at three different times $\frac{1}{3}t_f$, $\frac{2}{3}t_f$, t_f.*

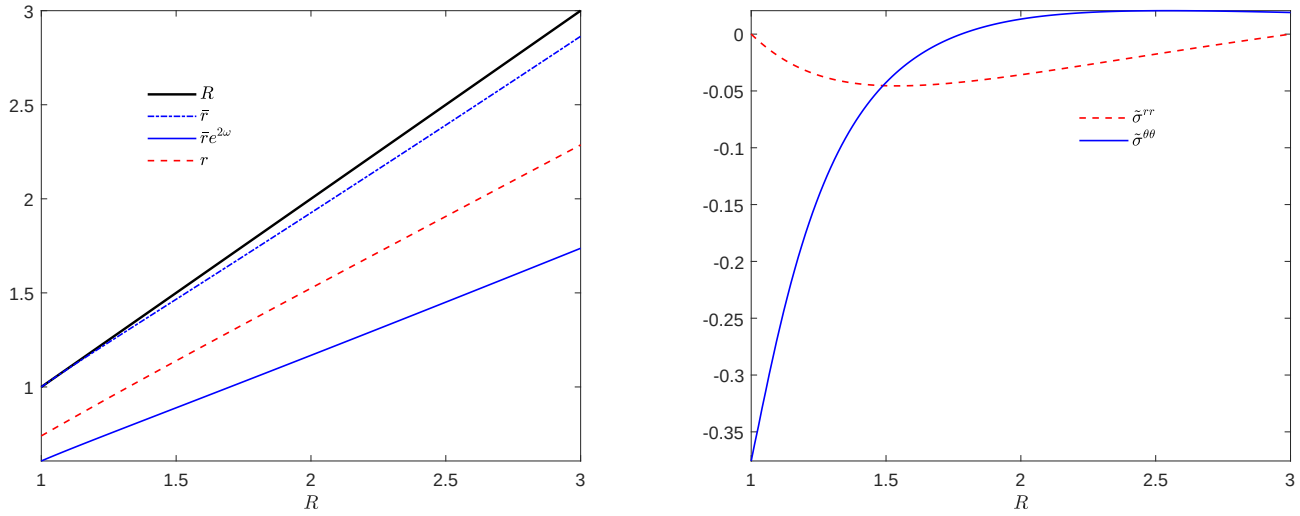

Figure 4: *Left: Time-independent quantities at the end of accretion. The radial coordinate R, the external radius at the time of attachment $\bar{r}(R)$, the "cooled-down" external radius at the time of attachment $e^{\omega(T_a)}\bar{r}(R)$ at the ambient temperature T_a, and the relaxed $\tilde{r}(R)$ corresponding to the residually stressed configuration. Right: Radial and circumferential residual stresses $\tilde{\sigma}^{rr}$ (red) and $\tilde{\sigma}^{\theta\theta}$ (blue). Note that $\tilde{\sigma}^{\theta\theta}$ is not a physical component, but is very close to $r^2\tilde{\sigma}^{\theta\theta}$ as its highest value is at $R = 1$. Note also that the values of both components of residual stress are comparable with the respective values of the thermal stresses during accretion shown in Fig. 3.*

3.4 Numerical results

In the numerical examples the growth velocity is assumed constant in time, i.e., $u(t) \equiv u$. This implies $S(t) = ut$ and $\tau(R) = \frac{R-R_0}{u}$. We take $L_o = R_0$, $T_o = T_m$, while growth is assumed to stop when the material external radius is $3L_o$. This implies that $u = 2L_o/t_o$. The values of all the parameters involved in the calculations are shown in Table 1, while plots of the numerical results are shown in Figs. 2, 3 and 4. Note that in the numerical examples we show the residually stressed configurations for which temperature is uniform. This means that

incompatibility (or residual stress) is not caused directly by thermal expansion/contraction. However, the residual stresses indirectly depend on the thermal strains during the accretion process thorugh the accretion tensor $\boldsymbol{Q}$, which depends on the history of deformation localized on the growth surface.

For the numerical calculations, we use a discrete time domain with a constant time interval h. In each time interval, we use a two-step numerical scheme based on the finite difference method to solve (17) and (22). The scheme is schematically illustrated in Fig. 5. We consider an equally distanced grid for R, and at the beginning of every time interval, we add a new point to the grid. At the time step $i-1$, a layer of hot material is added to the outer boundary of the cylinder. In the first step, we solve the thermal problem by discretizing (22) using the finite difference method. Let $\mathbf{T}$ be a vector containing the values of the temperature field T at all the grid points and let $\dot{\mathbf{T}} = \mathbf{F}(\mathbf{T})$ be the discretization of (22). We approximate the time derivative with an implicit backward Euler formula as $\mathbf{T}^{(i)} - \mathbf{T}^{(i-1)} = \mathsf{h}\mathbf{F}(\mathbf{T}^{(i)})$, where i is the time interval number. One can solve this equation with a linear solver to obtain $\mathbf{T}^{(i)}$, provided that $T^{(i)} = T_m$ at the new outer grid point, $\mathbf{T}^{(i-1)}$ is available from the previous time interval, and the boundary condition (23) is imposed at the grid point corresponding to $R = R_0$. In the second step, we use the same grid to discretize (17). Note that $\omega(T)$ in (17) is calculated using $\mathbf{T}^{(i)}$ obtained in step 1. Next, we impose $r(R_0) = R_0$, and from (13), $r_{,R} = 1$ at the outer grid point and use Newton's method to solve the discretization of (17) to obtain r at all the grid points. We use the values of r obtained in the previous time interval as the initial guess for Newton's method. We repeat the two steps for the next time interval. When we reach t_f, we remove the constraints, impose T_a everywhere, and calculate the residually-stressed configuration (see Fig. 4). We do this by using a load control procedure that gradually applies the change of material metric given by (16) multiplying $\boldsymbol{G}_0$ by $e^{2\boldsymbol{\omega}(T(R,t_f))} + \eta\left[e^{2\boldsymbol{\omega}(T_a)} - e^{2\boldsymbol{\omega}(T(R,t_f))}\right]$, as η increases form 0 to 1.

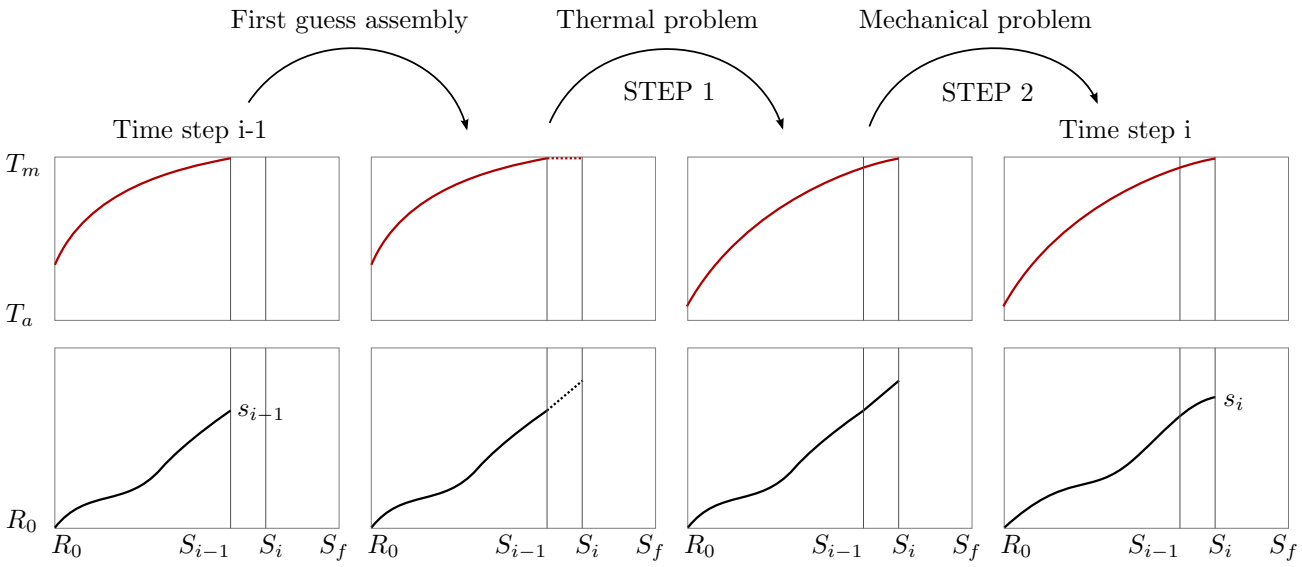

Figure 5: *A two-step computational scheme for a layered manufacturing process. The top row of plots represents the temperature $T(R)$. The bottom row of plots represents configuration $r(R)$. S_{i-1} is the external material radius at time t_{i-1}, S_i denotes the external material radius at time t_i, S_f is the external material radius at the final step t_f, s_{i-1} is the external deformed radius at time t_{i-1}, and s_i denotes the external deformed radius at time t_i.*

4 Accretion of a two-dimensional block

In this section, we consider the thermoelastic accretion of a two-dimensional block. We assume that the material starts being added on a rigid substrate. The initial width of the accreting body is L and might change in time due to finite deformations. The growing body is sitting in an ambient temperature T_a and the substrate is at temperature T_s, while stress-free layers of new material are continuously and uniformly added on the upper

boundary of the block at a temperature T_m. We assume that $T_a < T_m$ and $T_s < T_m$. This means that during the accretion process the growing body experiences deformations that are induced by differential thermal expansion. At time t, the material is added with a vertical flux of mass on the upper boundary of the body, which will constitute at each time the accretion surface ω_t.[9] The rate at which new material is added to the body at the time t is given by the scalar function $u(t)$. It should be emphasized that in the case of finite deformations the growth velocity is not necessarily normal to the growth surface throughout the accretion process. We neglect the effect of body forces and assume that the material is added in a stress-free state. We assume that the block is made of a uniform isotropic incompressible solid, with a uniform isotropic coefficient of thermal expansion $\alpha(T)$, and a uniform isotropic coefficient of heat conduction $K(T)$. We choose Cartesian coordinates (x, y) in the ambient space, so that the material is initially deposited on the line segment $[-\frac{L}{2}, \frac{L}{2}] \times \{0\}$ representing ω_0. The ambient metric $\boldsymbol{g}$ in Cartesian coordinates is represented by the diagonal matrix $\mathrm{diag}(1, 1)$.

4.1 The material manifold

We take a rectangle with a time-dependent height $S(t)$ as the material manifold, viz.

$$\mathcal{B}_t = \left\{ (X, Y) \in \mathbb{R}^2 \,\middle|\, -\frac{L}{2} \le X \le \frac{L}{2}\,,\ 0 \le Y \le S(t) \right\}.$$

In doing so we assume that the accretion process does not change the topology of the body. We define the time of attachment map $\tau = S^{-1}$, assigning to each layer of vertical coordinate $Y \ge 0$ its time of attachment $\tau(Y)$. Assuming that accretion starts at $t = 0$, it follows that $\tau(0) = 0$, and equivalently, $S(0) = 0$. The material growth velocity $\boldsymbol{U}(t)$ is then vertical and has norm $U(t) = u(t)$. This means that the thickness $U(t)\mathrm{d}t$ of the added ring in the material manifold is equal to the thickness $u(t)\mathrm{d}t$ of the added ring in the spatial manifold, as shown in Fig. 6. Therefore the height of $\mathcal{B}_t$ is $S(t) = \int_0^t u(\eta)\mathrm{d}\eta$. The material metric $\boldsymbol{G}$ will be taken consistently in order to obtain the Riemannian material manifold $(\mathcal{B}_t, \boldsymbol{G})$.

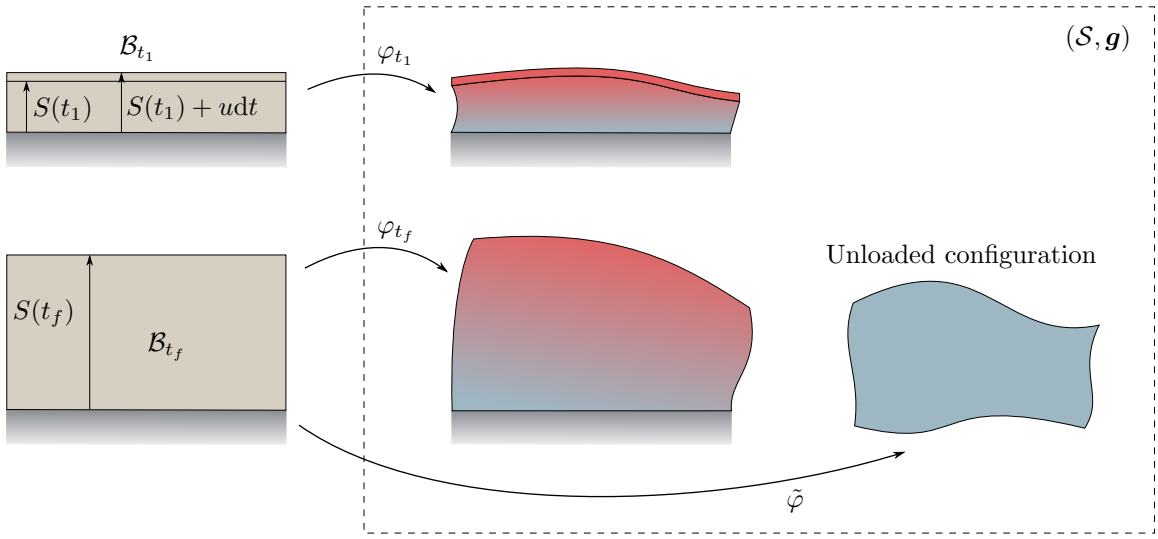

Figure 6: *Configurations of an accreting block.*

[9] It is assumed that throughout the whole accretion process the configuration of the accretion surface is given by points $(x, f(x, t))$, for some time-dependent f, so that the vertical addition of material on the whole upper boundary will always be possible.

4.2 Kinematics of the accreting body

Let (X, Y) and (x, y) be the Cartesian coordinates in the material manifold $\mathcal{B}_t$ and the ambient space $\mathcal{S}$, respectively. A motion for $\mathcal{B}_t$ is therefore a map $(x(X, Y, t), y(X, Y, t))$.[10] Remember that, given a configuration $\varphi_t : \mathcal{B}_t \to \mathcal{S}$ with tangent map $\boldsymbol{F}(t) = T\varphi_t$, the frozen deformation gradient field $\bar{\boldsymbol{F}}(X, Y) = \boldsymbol{F}(X, Y, \tau(Y))$ "freezes" the deformation gradient at the time of attachment of each layer. One can express $\bar{\boldsymbol{F}}$ as

$$\bar{\boldsymbol{F}} = \begin{bmatrix} \frac{\partial x}{\partial X} & \frac{\partial x}{\partial Y} \\ \frac{\partial y}{\partial X} & \frac{\partial y}{\partial Y} \end{bmatrix}_{t=\tau(Y)} . \tag{24}$$

Note that because the growth surface is traction free the material growth velocity is related to the spatial growth velocity as $\boldsymbol{u} = \bar{\boldsymbol{F}}\boldsymbol{U}$. Therefore, having assumed $U(t) = u(t)$, from (24) one obtains

$$\left.\frac{\partial x}{\partial Y}\right|_{t=\tau(Y)} = 0\,, \qquad \left.\frac{\partial y}{\partial Y}\right|_{t=\tau(Y)} = 1\,,$$

which is a two-dimensional analogue of (13). Thus, one can write Eq. (24) as

$$\bar{\boldsymbol{F}} = \begin{bmatrix} \left.\frac{\partial x}{\partial X}\right|_{t=\tau(Y)} & 0 \\ \left.\frac{\partial y}{\partial X}\right|_{t=\tau(Y)} & 1 \end{bmatrix} . \tag{25}$$

4.3 The material metric

After having chosen a suitable material configuration, one defines a metric $\boldsymbol{G}$, which depends on the temperature following (1) and (2) as $\boldsymbol{G} = e^{2\omega(T)}\boldsymbol{G}_0$, with the function ω such that $\omega(T_m) = 0$, and so $e^{2\omega(T_m)} = 1$. The metric $\boldsymbol{G}$ also takes into account the history of loading during the accretion process following (3) with $\boldsymbol{Q} = \bar{\boldsymbol{F}}$. Using the same coordinate charts as above and recalling Eq. (25), one obtains

$$\boldsymbol{G}_0 = \begin{bmatrix} \left.\frac{\partial x}{\partial X}\right|^2_{t=\tau(Y)} + \left.\frac{\partial y}{\partial X}\right|^2_{t=\tau(Y)} & \left.\frac{\partial y}{\partial X}\right|_{t=\tau(Y)} \\ \left.\frac{\partial y}{\partial X}\right|_{t=\tau(Y)} & 1 \end{bmatrix} , \tag{26}$$

and the temperature-dependent reads $\boldsymbol{G} = e^{2\omega}\boldsymbol{G}_0$.

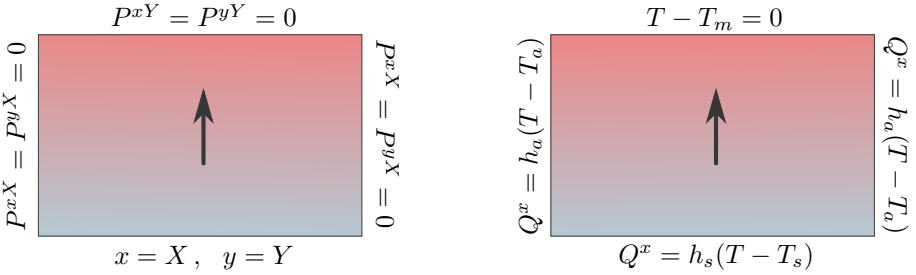

Figure 7: *Boundary conditions for the displacement and the stress (left), and for the temperature and the heat flux (right).*

4.4 Governing equations

We assume that the material is incompressible, i.e., $J = 1$, which by virtue of (5) can be written as

$$\sqrt{\frac{\det \boldsymbol{g}}{\det \boldsymbol{G}}}\det \boldsymbol{F} = \frac{\det \boldsymbol{F}}{\det \bar{\boldsymbol{F}}} e^{-\operatorname{tr}\boldsymbol{\omega}} = 1\,,$$

[10] Unlike the one-dimensional example of the axi-symmetric infinite cylinder, it is not possible to define $s(t)$ as the deformation is not uniform along the width of the block.

since $\boldsymbol{Q} = \bar{\boldsymbol{F}}$. Rearranging and emphasizing the dependence on the space coordinates and time, one has

$$\det \boldsymbol{F}(X, Y, t) = e^{2\omega(T(X,Y,t))} \det \bar{\boldsymbol{F}}(X, Y). \tag{27}$$

We write the balance of linear momentum in terms of the first Piola-Kirchhoff stress tensor which is convenient for imposing the boundary conditions. We consider a neo-Hookean model with a temperature-dependent μ (see Appendix A). The first Piola-Kirchhoff stress tensor can be written using (7) and (3) as

$$P^{aA} = \mu(T) F^a{}_B G^{AB} - p F^A{}_b g^{ab} = \mu(T) e^{2\omega(T)} F^a{}_B \bar{F}^A{}_c \bar{F}^B{}_b g^{bc} - p F^A{}_b g^{ab}\,. \tag{28}$$

We neglect the inertial effects as accretion is a slow process, and the balance of linear momentum is written as

$$\operatorname{Div} \boldsymbol{P} + \varrho_0 \mathbf{f} = \mathbf{0}\,. \tag{29}$$

The boundary conditions for the balance of linear momentum are shown in Fig. 7. Note that the material Christoffel symbols vanish since we are using Cartesian coordinates, and so the divergence of $\boldsymbol{P}$ in coordinates reads

$$P^{aA}{}_{|A} = P^{aA}{}_{,A} + \Gamma^A{}_{AC} P^{aC}\,,$$

where the Christoffel symbols $\Gamma^A{}_{BC}$ for $\nabla^{\boldsymbol{G}}$ can be computed from (26). Once accretion is completed, one can calculate the relaxed configuration $\tilde{\varphi}$ with residual stress $\tilde{\boldsymbol{P}}$ or $\tilde{\boldsymbol{\sigma}}$ by imposing uniform ambient temperature $T = T_a$ and traction-free boundary conditions.

The temperature field T that appears in the governing equations (27) and (28) is governed by Eq. (10). In the absence of external heat supply and neglecting the mechanical dissipation term, it reads

$$\rho c_E \dot{T} - \operatorname{Div}\left(K \boldsymbol{G}^{\sharp} \mathrm{d}T\right) = 0\,.$$

Using components and assuming a uniform K one obtains

$$\rho c_E \dot{T} - K G^{AB} \left(\frac{\partial^2 T}{\partial X^A \partial X^B} - \Gamma^C{}_{AB} \frac{\partial T}{\partial X^C} \right) = 0\,, \tag{30}$$

with the boundary conditions shown in Fig. 7.

Parameter	Symbol	Value	
Width in the reference configuration	L	$1\ L_o$	
Shear modulus	μ	$1\ \mu_o$	
Accretion time	t_f	$1\ t_o$	
Melting temperature	T_m	$1\ T_o$	
Thermal expansion coefficient at T_a	α_a	$0.2\ T_o^{-1}$	
		Case 1	Case 2
Ambient temperature	T_a	$0.5\ T_o$	$0\ T_o$
Substrate temperature	T_s	$0\ T_o$	$0.5\ T_o$
Diffusivity coefficient	D	$0.2\ \frac{L_o^2}{t_o}$	$1\ \frac{L_o^2}{t_o}$
Heat transfer coefficient (ambient)	h_a	$10 \frac{\mu_o L_o}{t_o T_o}$	$1 \frac{\mu_o L_o}{t_o T_o}$
Heat transfer coefficient (substrate)	h_s	$1 \frac{\mu_o L_o}{t_o T_o}$	$10 \frac{\mu_o L_o}{t_o T_o}$

Table 2: *Parameters of the accreting two-dimensional block. Note that the diffusivity coefficient is defined as* $D = \frac{K}{\rho_0 c_E}$.

4.5 Numerical results

In the numerical examples the growth velocity is assumed constant, i.e., $u(t) \equiv u$. This implies that $S(t) = ut$ and $\tau(Y) = Y/u$. We take $S(t_f) = L_o$, and therefore, $u = L_o/t_o$. As in the previous example, the reference

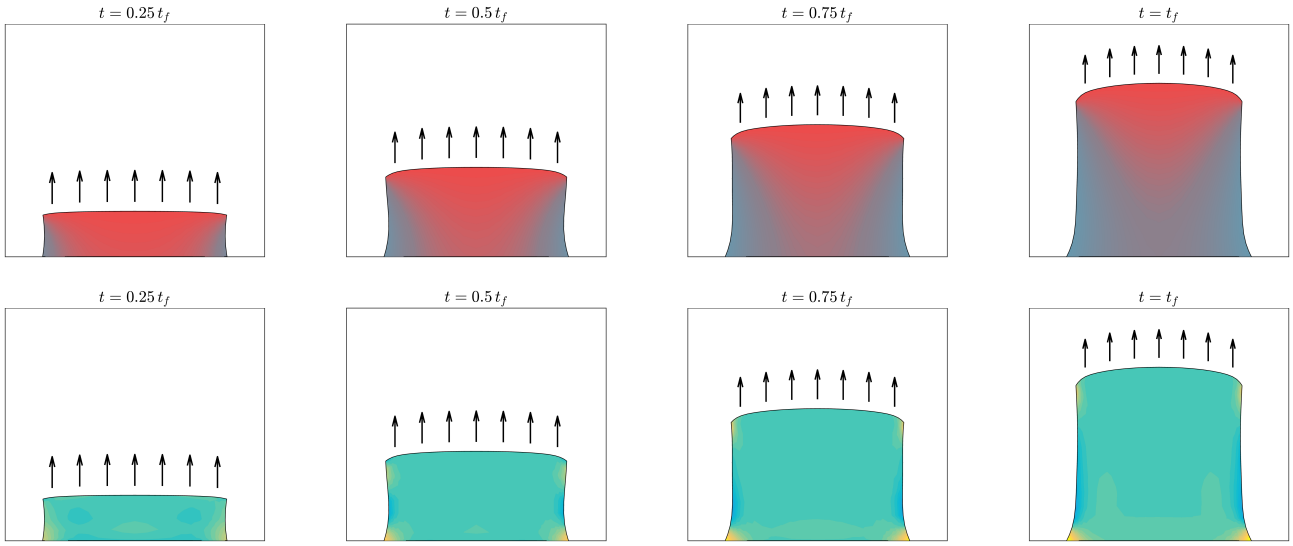

Figure 8: *The accreting block at four different times* $\frac{1}{4}t_f$, $\frac{1}{2}t_f$, $\frac{3}{4}t_f$, t_f. *The colors show temperature (top) and* $\operatorname{tr}\boldsymbol{C}$ *(bottom), lighter colors correspond to higher values. The plots correspond to Case 1: the heat flux is driven by the heat exchange with the lateral sides of the block, as can be observed from the temperature contour.*

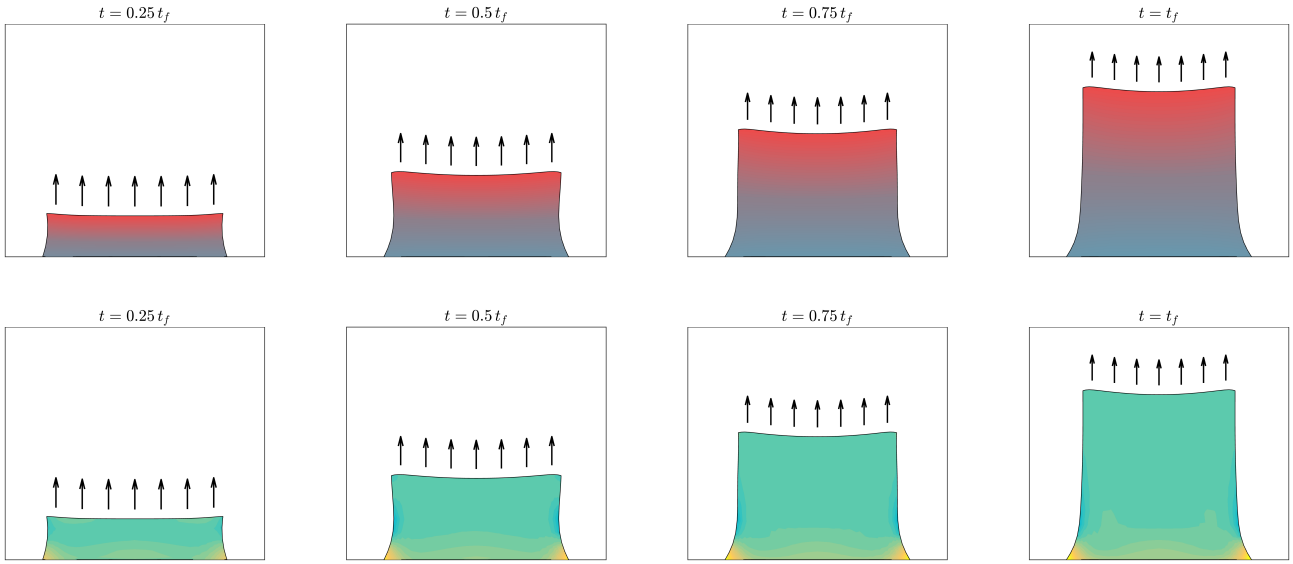

Figure 9: *The accreting block at four different times* $\frac{1}{4}t_f$, $\frac{1}{2}t_f$, $\frac{3}{4}t_f$, t_f. *The colors show temperature (top) and* $\operatorname{tr}\boldsymbol{C}$ *(bottom), lighter colors correspond to higher values. The plots correspond to Case 2: the heat flux is driven by the heat exchange with the rigid substrate at the bottom side of the block, as can be observed from the temperature contour.*

temperature T_o is the melting temperature T_m. We solve the same problem using two different sets of thermal parameters. In the first case (Figs. 8 and 10) the heat flux is driven by heat exchange with the sides of the block, while in the second case (Figs. 9 and 10) the body is cooled down mainly by the lower side that is in contact with the substrate. Note that for incompressible two-dimensional solids $\operatorname{tr}\boldsymbol{C}$ characterizes $\boldsymbol{C}$ as the other invariant is $\det\boldsymbol{C} = 1$. The values of all the parameters involved in the calculations are given in Table 2.

Here we use an approach similar to that of §3.4, but with a more sophisticated discretization method that is suitable for 2D problems. To approximate the temperature and deformation history of a body in a

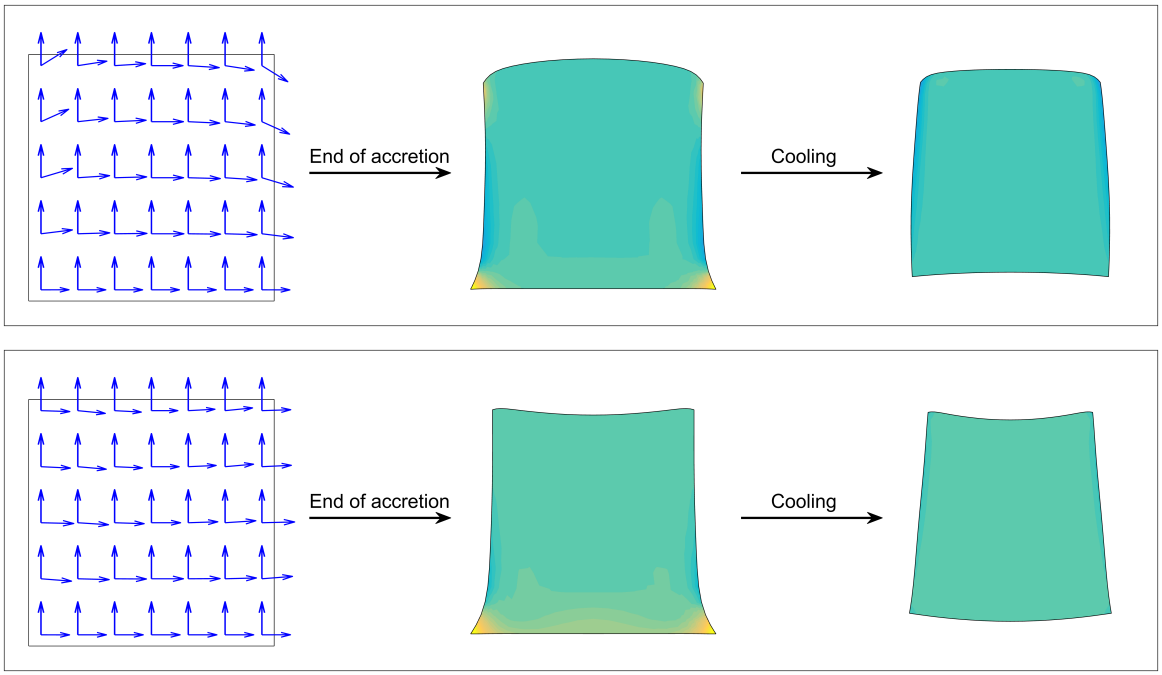

Figure 10: *Top: The heat flux is driven by the heat exchange with the lateral sides of the block (Case 1). Bottom: The heat flux is driven by the heat exchange with the rigid substrate at the bottom side of the block (Case 2). Left: The material manifold—an $L \times ut_f$ rectangle—with the field of frames representing the Cartesian frame $\{\boldsymbol{i}, \boldsymbol{j}\}$ deformed by $\bar{\boldsymbol{F}}$, i.e., the moving frame $\{\bar{\boldsymbol{F}}\boldsymbol{i}, \bar{\boldsymbol{F}}\boldsymbol{j}\}$. In this example the two-point tensor $\bar{\boldsymbol{F}}$ is the analogue of the plastic part of the deformation gradient in multiplicative plasticity. Center: The configuration at the final time of accretion t_f. Right: The residually-stressed configuration after thermal and mechanical relaxation, i.e., relative to the uniform temperature $T = T_a$ and traction-free boundary conditions. Note that the residually-stressed configurations in the two cases are completely different.*

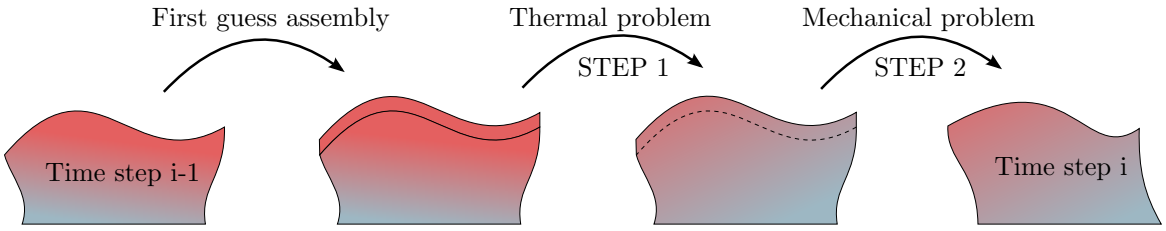

Figure 11: *A two-step computational scheme for a layered manufacturing process.*

layered manufacturing process, we discretize the time domain into a finite set of equal time intervals h and design a two-step numerical scheme for each time interval (see Fig. 11). In the first step, we assume that a layer of new hot material is added to the initial body. We update the grid points and assign to the new layer a metric $\boldsymbol{G}_0$ as in (26), where x and y are available from the time step $i-1$. Note that since the new layer is at temperature T_m, the material metric $\boldsymbol{G}$ is exactly $\boldsymbol{G}_0$. Next, we solve the heat equation (30) to obtain the temperature field on the entire body (old layers and the newly added layer) after one time interval. Following our approach in §3.4, let $\dot{\mathsf{T}} = \mathsf{F}(\mathsf{T})$ be the discretization of (30), where T is an array containing the values of the temperature field T at all points of a two-dimensional grid. The implicit backward Euler formula gives $\mathsf{T}^{(i)} - \mathsf{T}^{(i-1)} = \mathsf{h}\mathsf{F}(\mathsf{T}^{(i)})$. Note that the grid points have been updated after adding the new layer, and thus, we interpolate $\mathsf{T}^{(i-1)}$ on the new grid points. We choose the interpolated $\mathsf{T}^{(i-1)}$ as the initial guess of Newton's method for $\mathsf{T}^{(i)}$. Then, to obtain $\mathsf{T}^{(i)}$, we impose the boundary conditions and solve the above equation using Newton's method considering a numerical Jacobian matrix. In the second step, we use the computed temperature $\mathsf{T}^{(i)}$ to update the temperature-dependent material metric $\boldsymbol{G}$ and then numerically solve

the equations of nonlinear elasticity (29) subjected to change of $\boldsymbol{G} = e^{2\omega}\boldsymbol{G}_0$ with $\boldsymbol{G}_0$ given in (26). This gives us the deformed configuration of the body after adding a layer of new hot material. We assume for simplicity that the boundary of the body $\partial_D\mathcal{B}_t$ is a disjoint union of $\partial_D\mathcal{B}_t$ and $\partial_N\mathcal{B}_t$ and is subjected to the boundary conditions $\varphi_t = \hat{\varphi}_t$ on $\partial_D\mathcal{B}_t$ and $\boldsymbol{P}\boldsymbol{N} = \boldsymbol{t}$ on $\partial_N\mathcal{B}_t$, where $\boldsymbol{N}$ is the unit outward normal vector field of $\partial_N\mathcal{B}_t$. For the numerical calculations, we use the following weak formulation of (29)

$$
\begin{aligned}
&\int_{\mathcal{B}_t} \Upsilon^a{}_{|B} P_a{}^B \,\mathrm{d}V = \int_{\mathcal{B}_t} \varrho_0 b_a \Upsilon^a \,\mathrm{d}V + \int_{\partial_N\mathcal{B}_t} t_a \Upsilon^a \,\mathrm{d}A\,,\\
&\int_{\mathcal{B}_t} (J-1) q \,\mathrm{d}V = 0\,,\\
&\varphi_t = \hat{\varphi} \text{ on } \partial_D\mathcal{B}_t\,,
\end{aligned}
\tag{31}
$$

where $\boldsymbol{\Upsilon}$ is an arbitrary vector field such that $\boldsymbol{\Upsilon} = \boldsymbol{0}$ on $\partial_D\mathcal{B}_t$, and q is an arbitrary scalar field. Also, recall that $\boldsymbol{P}$ is given by (28). Next, we discretize (31) using a variational differential quadrature (VDQ) method [Faghih Shojaei and Ansari, 2017] and obtain a set of algebraic equations. The 2D domain is discretized by Chebyshev-Gauss-Lobatto grid points along the two axes. Over the entire 2D grid points, the derivatives in (31) are approximated using the generalized differential quadrature (GDQ) method [Shu, 2012] and the integrals are approximated by the relation given in [Faghih Shojaei and Ansari, 2017, Appendix b]. The boundary conditions in $(31)_3$ are imposed using the standard elimination approach. At time step i, the discretized material metric $\mathbf{G}^{(i)}$ changes due to the new distribution of temperature $\mathbf{T}^{(i)}$. We use Newton's method to solve the resulting algebraic equations from (31) in a load control procedure that gradually applies the change of material metric by $\mathbf{G}^{(i-1)} + \eta[\mathbf{G}^{(i)} - \mathbf{G}^{(i-1)}]$ as η increases form 0 to 1. We observed that using the same grid points for approximating the spatial coordinates (x, y) and the pressure p results in a singular method. This is due to violation of Ladyzhenskaya-Babuška-Brezzi (LBB) condition. To overcome this issue, we used a coarser grid for approximating p relative to that of (x, y). To improve the efficiency, we calculate the Jacobian matrix analytically by linearizing (31). We repeat the two steps for the next time interval.

5 Conclusions

In this paper we formulated a theory for the coupling of accretion and thermoelasticity. We focused on the analytical formulation of the thermoelastic accretion of an infinite cylinder and of a two-dimensional body. These two examples represent very simple one-dimensional and two-dimensional benchmark problems for thermoelastic accretion. We developed numerical schemes for the solution of these two problems. The numerical calculations allowed us to uncover the general features of accretion in the context of thermally induced deformations, such as the presence of residual stress. The numerical calculations allowed us to show the main features of thermal accretion, e.g., the presence of residual stress in accreted bodies, and the dependence of their final characteristics on the history of deformation. This in turn implies the dependence of the mechanical characteristics of an accreted body on the parameters of the accretion process. In particular, in the two-dimensional case, changing the boundary conditions for the heat equation, we were able to show the strong dependence of the characteristics of the accreted body on the thermal parameters of accretion. This suggests a new approach to control accretion through tailoring the thermal parameters in order to achieve specific mechanical characteristics.

Extending the present theory to include changes of phase will be the subject of a future communication. As a matter of fact, solidification represents a very important example of accretion, and to the best of our knowledge, the nonlinear Stefan problem of a body undergoing large deformations has not been studied to this date. As we mentioned earlier, it would be interesting to see how one can design specific accretion processes in order to achieve desired shapes and mechanical properties in an accreted body. This could be done through the manipulation of parameters such as growth velocity, heat transfer coefficients, ambient temperature, etc. A further extension of the present work would be the development of an efficient finite element framework that can be used to simulate more complex accretion problems. In particular, one can modify (31) by considering $\boldsymbol{F}$ and $\boldsymbol{P}$ as independent variables and use the mixed finite element methods for compressible and incompressible nonlinear elasticity introduced in [Faghih Shojaei and Yavari, 2018, 2019] to solve accretion problems. Finally, it would be interesting to consider different ways of addition of material in order to address additive manufacturing processes more specifically.

Acknowledgement

This research was supported by NSF–Grant No. CMMI 1130856 and ARO W911NF-18-1-0003.

References

R. Abi-Akl, R. Abeyaratne, and T. Cohen. Kinetics of surface growth with coupled diffusion and the emergence of a universal growth path. *Proceedings of the Royal Society A*, 475(2221):20180465, 2019.

H. Bikas, P. Stavropoulos, and G. Chryssolouris. Additive manufacturing methods and modelling approaches: a critical review. *The International Journal of Advanced Manufacturing Technology*, 83(1-4):389–405, 2016.

P. Chadwick. Thermo-mechanics of rubberlike materials. *Philosophical Transactions of the Royal Society of London. Series A, Mathematical and Physical Sciences*, 276(1260):371–403, 1974.

S. Dadbakhsh, L. Hao, and N. Sewell. Effect of selective laser melting layout on the quality of stainless steel parts. *Rapid Prototyping Journal*, 18(3):241–249, 2012.

B. de La Batut, O. Fergani, V. Brotan, M. Bambach, and M. El Mansouri. Analytical and numerical temperature prediction in direct metal deposition of Ti6Al4V. *Journal of Manufacturing and Materials Processing*, 1(1): 3, 2017.

E. R. Denlinger and P. Michaleris. Mitigation of distortion in large additive manufacturing parts. *Proceedings of the Institution of Mechanical Engineers, Part B: Journal of Engineering Manufacture*, 231(6):983–993, 2017.

E. R. Denlinger, J. C. Heigel, and P. Michaleris. Residual stress and distortion modeling of electron beam direct manufacturing ti-6al-4v. *Proceedings of the Institution of Mechanical Engineers, Part B: Journal of Engineering Manufacture*, 229(10):1803–1813, 2015.

O. W. Dillon Jr. A nonlinear thermoelasticity theory. *Journal of the Mechanics and Physics of Solids*, 10(2): 123–131, 1962.

M. Epstein and G. A. Maugin. Thermomechanics of volumetric growth in uniform bodies. *International Journal of Plasticity*, 16(7-8):951–978, 2000.

M. Faghih Shojaei and R. Ansari. Variational differential quadrature: a technique to simplify numerical analysis of structures. *Applied Mathematical Modelling*, 49:705–738, 2017.

M. Faghih Shojaei and A. Yavari. Compatible-strain mixed finite element methods for incompressible nonlinear elasticity. *Journal of Computational Physics*, 361:247 – 279, 2018.

M. Faghih Shojaei and A. Yavari. Compatible-strain mixed finite element methods for 3D compressible and incompressible nonlinear elasticity. *Computer Methods in Applied Mechanics and Engineering*, 357:112610, 2019.

O. Fergani, F. Berto, T. Welo, and S. Liang. Analytical modelling of residual stress in additive manufacturing. *Fatigue & Fracture of Engineering Materials & Structures*, 40:971–978, 2017.

W. E. Frazier. Direct digital manufacturing of metallic components: vision and roadmap. In *21st Annual International Solid Freeform Fabrication Symposium, Austin, TX, Aug*, pages 9–11, 2010.

W. E. Frazier. Metal additive manufacturing: A review. *Journal of Materials Engineering and Performance*, 23(6):1917–1928, 2014.

J.-F. Ganghoffer and I. Goda. A combined accretion and surface growth model in the framework of irreversible thermodynamics. *International Journal of Engineering Science*, 127:53–79, 2018.

K. Garikipati, E. M. Arruda, K. Grosh, H. Narayanan, and S. Calve. A continuum treatment of growth in biological tissue: the coupling of mass transport and mechanics. *Journal of the Mechanics and Physics of Solids*, 52(7):1595–1625, 2004.

S. Ghosh and J. Choi. Three-dimensional transient finite element analysis for residual stresses in the laser aided direct metal/material deposition process. *Journal of Laser Applications*, 17(3):144–158, 2005.

I. Gibson, D. Rosen, and B. Stucker. *Additive Manufacturing Technologies: 3D Printing, Rapid Prototyping, and Direct Digital Manufacturing*. SpringerLink : Bücher. Springer New York, 2014.

A. Goriely. *The Mathematics and Mechanics of Biological Growth*, volume 45. Springer, 2017.

D. Gu, W. Meiners, K. Wissenbach, and R. Poprawe. Laser additive manufacturing of metallic components: materials, processes and mechanisms. *International Materials Reviews*, 57(3):133–164, 2012.

N. Hodge, R. Ferencz, and J. Solberg. Implementation of a thermomechanical model for the simulation of selective laser melting. *Computational Mechanics*, 54(1):33–51, 2014.

N. Hodge, R. Ferencz, and R. Vignes. Experimental comparison of residual stresses for a thermomechanical model for the simulation of selective laser melting. *Additive Manufacturing*, 12:159–168, 2016.

G. Holzapfel and J. Simo. Entropy elasticity of isotropic rubber-like solids at finite strains. *Computer Methods in Applied Mechanics and Engineering*, 132(1):17–44, 1996.

T. J. Horn and O. L. Harrysson. Overview of current additive manufacturing technologies and selected applications. *Science Progress*, 95(3):255–282, 2012.

H. Hu and S. A. Argyropoulos. Mathematical modelling of solidification and melting: a review. *Modelling and Simulation in Materials Science and Engineering*, 4(4):371, 1996.

S. H. Huang, P. Liu, A. Mokasdar, and L. Hou. Additive manufacturing and its societal impact: A literature review. *The International Journal of Advanced Manufacturing Technology*, 67:1–13, 2013.

N. W. Klingbeil, J. L. Beuth, R. Chin, and C. Amon. Residual stress-induced warping in direct metal solid freeform fabrication. *International Journal of Mechanical Sciences*, 44(1):57–77, 2002.

G. N. Levy, R. Schindel, and J.-P. Kruth. Rapid manufacturing and rapid tooling with layer manufacturing (lm) technologies, state of the art and future perspectives. *CIRP Annals-Manufacturing Technology*, 52(2): 589–609, 2003.

C. Li, C. Fu, Y. Guo, and F. Fang. A multiscale modeling approach for fast prediction of part distortion in selective laser melting. *Journal of Materials Processing Technology*, 229:703–712, 2016.

Y. Li and D. Gu. Thermal behavior during selective laser melting of commercially pure titanium powder: Numerical simulation and experimental study. *Additive Manufacturing*, 1:99–109, 2014.

L.-E. Loh, C.-K. Chua, W.-Y. Yeong, J. Song, M. Mapar, S.-L. Sing, Z.-H. Liu, and D.-Q. Zhang. Numerical investigation and an effective modelling on the selective laser melting (slm) process with aluminium alloy 6061. *International Journal of Heat and Mass Transfer*, 80:288–300, 2015.

J. Marsden and T. Hughes. *Mathematical Foundations of Elasticity*. Dover Civil and Mechanical Engineering Series. Dover, 1983.

M. Matsumoto, M. Shiomi, K. Osakada, and F. Abe. Finite element analysis of single layer forming on metallic powder bed in rapid prototyping by selective laser processing. *International Journal of Machine Tools and Manufacture*, 42(1):61–67, 2002.

P. Mercelis and J.-P. Kruth. Residual stresses in selective laser sintering and selective laser melting. *Rapid Prototyping Journal*, 12(5):254–265, 2006.

P. Michaleris. Modeling metal deposition in heat transfer analyses of additive manufacturing processes. *Finite Elements in Analysis and Design*, 86:51–60, 2014.

R. Ogden. Large deformation isotropic elasticity: on the correlation of theory and experiment for compressible rubberlike solids. *Proceedings of the Royal Society of London A*, 328(1575):567–583, 1972a.

R. Ogden. Large deformation isotropic elasticity: on the correlation of theory and experiment for incompressible rubberlike solids. *Proceedings of the Royal Society of London. A. Mathematical and Physical Sciences*, 326 (1567):565–584, 1972b.

R. Ogden. On the thermoelastic modeling of rubberlike solids. *Journal of Thermal Stresses*, 15(4):533–557, 1992.

A. Ozakin and A. Yavari. A geometric theory of thermal stresses. *Journal of Mathematical Physics*, 51(3): 032902, 2010.

O. Richmond and R. Tien. Theory of thermal stresses and air-gap formation during the early stages of solidification in a rectangular mold. *Journal of the Mechanics and Physics of Solids*, 19(5):273–284, 1971.

J. Rifkin. *The Third Industrial Revolution: How Lateral Power Is Transforming Energy, the Economy, and the World*. St. Martin's Press, 2011.

S. Sadik and A. Yavari. Geometric nonlinear thermoelasticity and the time evolution of thermal stresses. *Mathematics and Mechanics of Solids*, 22(7):1546–1587, 2017.

K. Schwerdtfeger, M. Sato, and K.-H. Tacke. Stress formation in solidifying bodies. solidification in a round continuous casting mold. *Metallurgical and Materials Transactions B*, 29(5):1057–1068, 1998.

N. Shamsaei, A. Yadollahi, L. Bian, and S. M. Thompson. An overview of direct laser deposition for additive manufacturing; part ii: Mechanical behavior, process parameter optimization and control. *Additive Manufacturing*, 8:12–35, 2015.

M. Shiomi, K. Osakada, K. Nakamura, T. Yamashita, and F. Abe. Residual stress within metallic model made by selective laser melting process. *CIRP Annals-Manufacturing Technology*, 53(1):195–198, 2004.

C. Shu. *Differential Quadrature and its Application in Engineering*. Springer Science & Business Media, 2012.

F. Sozio and A. Yavari. Nonlinear mechanics of surface growth for cylindrical and spherical elastic bodies. *Journal of the Mechanics and Physics of Solids*, 98:12 – 48, 2017.

F. Sozio and A. Yavari. Nonlinear mechanics of accretion. *Journal of Nonlinear Science*, 29(4):1813–1863, 2019a.

F. Sozio and A. Yavari. Riemannian and Euclidean material structures in anelasticty. *Mathematics and Mechanics of Solids*, 2019b. doi: 10.1177/1081286519884719.

J. Stefan. Über einge problem der theoric der wärmeleitung. *Sitzber. Wien Akad. Mat. Natur*, 98:173–484, 1989.

D. Swain and A. Gupta. Biological growth in bodies with incoherent interfaces. *Proceedings of the Royal Society A: Mathematical, Physical and Engineering Sciences*, 474(2209):20170716, 2018.

S. M. Thompson, L. Bian, N. Shamsaei, and A. Yadollahi. An overview of direct laser deposition for additive manufacturing; part i: Transport phenomena, modeling and diagnostics. *Additive Manufacturing*, 8:36–62, 2015.

G. Tomassetti, T. Cohen, and R. Abeyaratne. Steady accretion of an elastic body on a hard spherical surface and the notion of a four-dimensional reference space. *Journal of the Mechanics and Physics of Solids*, 96: 333–352, 2016.

C. Truesdell and W. Noll. *The Non-Linear Field Theories of Mechanics*. Springer, third edition, 2004.

L. Truskinovsky and G. Zurlo. Nonlinear elasticity of incompatible surface growth. *Physical Review E*, 99(5): 053001, 2019.

R. Viskanta. Heat transfer during melting and solidification of metals. *ASME, Transactions, Journal of Heat Transfer*, 110:1205–1219, 1988.

C. Weller, R. Kleer, and F. T. Piller. Economic implications of 3d printing: Market structure models in light of additive manufacturing revisited. *International Journal of Production Economics*, 164:43–56, 2015.

A. Yavari. A geometric theory of growth mechanics. *Journal of Nonlinear Science*, 20(6):781–830, 2010.

M. F. Zaeh and G. Branner. Investigations on residual stresses and deformations in selective laser melting. *Production Engineering*, 4(1):35–45, 2010.

Appendices

A A nonlinear thermoelastic constitutive model

In this appendix, we present a thermoelastic model following the works of Chadwick [1974], Ogden [1972a,b, 1992], and Holzapfel and Simo [1996]. See [Sadik and Yavari, 2017] for more details. For a homogeneous isotropic solid, we denote by κ_0, μ_0 and β_0, the bulk modulus, the shear modulus, and the volumetric coefficient of thermal expansion at T_0, respectively, with $\beta(X,T)=\frac{\partial}{\partial T}\operatorname{tr}\boldsymbol{\omega}(X,T)$, while in the isotropic case $\beta(X,T)=3\frac{\partial}{\partial T}\omega(X,T)=3\alpha(X,T)$ in 3D, and $\beta(X,T)=2\frac{\partial}{\partial T}\omega(X,T)=2\alpha(X,T)$ in 2D. We consider the following constitutive model

$$\bar{\mathcal{W}}(T,\tilde{I},J)=\frac{\mu_0}{2}\frac{T}{T_0}(\tilde{I}-3)+\frac{\kappa_0}{2}\frac{T}{T_0}(J-1)^2-\kappa_0\beta_0(J-1)\,(T-T_0)-\rho\int_{T_0}^{T}c_E(\eta)\frac{T-\eta}{\eta}\mathrm{d}\eta\,,$$

where $\tilde{I}=J^{-2/3}I$, $I=\operatorname{tr}\boldsymbol{C}$, $J=\sqrt{\det\boldsymbol{C}}$, and c_E is the specific heat capacity at constant strain. In the incompressible case, we have the constraint $J=1$ associated with the pressure field p as the Lagrange multiplier and the constitutive model transforms to read

$$\bar{\mathcal{W}}(T,I)=\frac{\mu_0}{2}\frac{T}{T_0}(I-3)-\rho\int_{T_0}^{T}c_E(\eta)\frac{T-\eta}{\eta}\mathrm{d}\eta\,,$$

plus the Lagrange multiplier part $p(J-1)^2$. Note that the shear modulus is linear in temperature, i.e.,

$$\mu(T)=\mu_0\frac{T}{T_0}\,.$$

The simplest thermoelastic model for the expansion coefficients is given by a constant α, viz.

$$\alpha(T)=\alpha_0\,,\qquad \omega(T)=\omega_0\frac{T}{T_0}\,,\qquad \omega_0=\alpha_0T_0\,.$$

B A remark on the material metric

Eq. (1) is a generalization of the isotropic case that appeared in [Ozakin and Yavari, 2010]. In section 2.1 of [Sadik and Yavari, 2017], due to a mis-manipulation of the musical operators for raising and lowering indices, the representation of the material metric using the $\binom{1}{1}$-tensor $\boldsymbol{\omega}$ was mistakenly presented as

$$\boldsymbol{G}(X,T)=\boldsymbol{G}_0(X)e^{2\boldsymbol{\omega}(X,T)}.$$

Indeed, this representation may violate the symmetry requirement for the Riemannian metric $\boldsymbol{G}$, while the representation (1) ensures its symmetry. In what follow, we provide a correction of the proof appearing in section 2.1 of [Sadik and Yavari, 2017]. The manifold $(\mathcal{B},\boldsymbol{G}_0)$—which corresponds to the stress-free temperature field $T_0=T_0(X)$—is flat. Hence, there exists a local coordinate chart $\{Y^A\}$ in which

$$\boldsymbol{G}_0=\delta_{AB}\mathrm{d}Y^A\otimes\mathrm{d}Y^B.$$

Following Ozakin and Yavari [2010], the temperature-dependent material metric can be written as

$$\boldsymbol{G}(X,T) = \sum_K e^{2\omega_K(X,T)} \mathrm{d}Y^K \otimes \mathrm{d}Y^K,$$

where $\{\omega_A\}_{A=1,2,3}$ describes the thermal expansion properties of the material such that ω_K is related to the thermal expansion coefficient α_K in the direction $\frac{\partial}{\partial Y^K}$ by

$$\alpha_K(X,T) = \frac{\partial \omega_K}{\partial T}(X,T),$$

and $\omega_K(X,T_0) = 0$. Let the change of basis between $\{Y^A\}_{A=1,2,3}$ and some arbitrary local coordinate chart $\{X^A\}_{A=1,2,3}$ be written as

$$\mathrm{d}Y^K = A^K{}_J \mathrm{d}X^J,$$

which also reads as

$$\frac{\partial}{\partial Y^K} = (A^{-1})^I{}_K \frac{\partial}{\partial X^I}.$$

Then it follows that

$$\boldsymbol{G} = \left(\sum_K e^{2\omega_K} A^K{}_I A^K{}_J \right) \mathrm{d}X^I \otimes \mathrm{d}X^J.$$

Let $\boldsymbol{\omega}$ be the $\binom{1}{1}$-tensor

$$\boldsymbol{\omega} = \sum_K \omega_K \frac{\partial}{\partial Y^K} \otimes \mathrm{d}Y^K = \sum_K (A^{-1})^I{}_K \omega_K A^K{}_J \frac{\partial}{\partial X^I} \otimes \mathrm{d}X^J.$$

However, in $\{X^A\}$, one has

$$\boldsymbol{G}_0 = \delta_{AB} A^A{}_I A^B{}_J \mathrm{d}X^I \otimes \mathrm{d}X^J.$$

Hence, the material metric transforms to

$$\boldsymbol{G}(X,T) = e^{\omega^L{}_I} (G_0)_{LM}\, e^{\omega^M{}_J} \mathrm{d}X^I \otimes \mathrm{d}X^J,$$

where $(G_0)_{LM}$ are the components of $\boldsymbol{G}_0$ in $\{X^A\}$. This is the coordinate representation of (1). Note that even though the general representation for the material metric used in [Sadik and Yavari, 2017] had this symmetry fallacy, the results of the paper and the examples were not affected and remain valid.

C Christoffel symbols for the accreting cylinder

First note that denoting with $(\Gamma_0)^A{}_{BC}$ the Christoffel symbols relative to $\boldsymbol{G}_0$ as in (3), one obtains

$$\Gamma^A{}_{BC} = (\Gamma_0)^A{}_{BC} + (G_0)^{AD}[(G_0)_{DB}\omega_{,C} + (G_0)_{DC}\omega_{,B} - (G_0)_{BC}\omega_{,D}]\,.$$

Therefore, as $\boldsymbol{G}_0^\sharp : \boldsymbol{G}_0 = \dim \mathcal{B}$, one has

$$\Gamma^B{}_{BC} = (\Gamma_0)^B{}_{BC} + (\dim \mathcal{B})\ \omega_{,C}\,.$$

Under the assumption of a uniform material one has $\omega_{,C} = \frac{\partial \omega}{\partial T} T_{,C} = \alpha\, T_{,C}$, i.e., $\mathrm{d}\omega = \alpha\, \mathrm{d}T$, so one writes

$$\Gamma^B{}_{BC} = (\Gamma_0)^B{}_{BC} + (\dim \mathcal{B})\alpha\, T_{,C}\,.$$

Now we compute the Christoffel symbols for the material metric $\boldsymbol{G}$ of (16). The only non-zero Christoffel symbols are

$$\begin{aligned}
\Gamma^R{}_{RR} &= T_{,R}\alpha(T)\,,\\
\Gamma^R{}_{\Theta\Theta} &= -\bar{r}(R)\left[\bar{r}'(R) + \bar{r}(R)T_{,R}\alpha(T)\right]\,,\\
\Gamma^\Theta{}_{R\Theta} &= \frac{\bar{r}'(R)}{\bar{r}(R)} + T_{,R}\alpha(T)\,.
\end{aligned}$$

Now one can compute the material divergence $\mathrm{Div}[K(T)\boldsymbol{G}^{\sharp}\mathrm{d}T]$ for the heat equation as

$$\begin{aligned}
\mathrm{Div}[K(T)\boldsymbol{G}^{\sharp}\mathrm{d}T] &= \left[K(T)G^{AB}T_{,B}\right]_{|A} \\
&= \left[K(T)G^{AB}\right]_{|A}T_{,B} + K(T)G^{AB}\left[T_{,B}\right]_{|A} \\
&= \left[K(T)\right]_{|A}G^{AB}T_{,B} + K(T)G^{AB}\left[T_{,AB} - \Gamma^{C}{}_{AB}T_{,C}\right] \\
&= \frac{\mathrm{d}K}{\mathrm{d}T}T_{,R}{}^{2}G^{RR} + K(T)\left[T_{,RR}G^{RR} - \left(\Gamma^{R}{}_{RR}G^{RR} + \Gamma^{R}{}_{\Theta\Theta}G^{\Theta\Theta}\right)T_{,R}\right] \\
&= \left[\frac{\mathrm{d}K}{\mathrm{d}T}T_{,R}{}^{2} + \frac{K(T)}{\bar{r}(R)}\frac{\partial}{\partial R}\left(\bar{r}(R)\frac{\partial T}{\partial R}\right)\right]e^{-2\omega(T)}\,.
\end{aligned}$$

D The reduced form of the Clausius-Duhem inequality in thermoelastic accretion

In this appendix we discuss the restrictions that the second law of thermodynamics imposes on constitutive equations. In particular, we correct a mistake in [Sadik and Yavari, 2017],[11] which fortunately did not affect any of the results or conclusions of that work. The localized form of the Clausius-Duhem inequality reads

$$\rho\dot{\mathcal{N}} \geq \rho\frac{R}{T} - \mathrm{Div}\left(\frac{\boldsymbol{H}}{T}\right) + \rho\frac{\partial\mathcal{N}}{\partial\boldsymbol{G}}:\dot{\boldsymbol{G}}\,, \tag{32}$$

where $\mathcal{N} = \mathcal{N}(X, T, \boldsymbol{C}^{\flat}, \boldsymbol{G})$ is the specific entropy. Expanding Eq.(32) and multiplying by $T > 0$ one obtains

$$\rho T\left(\frac{\partial\mathcal{N}}{\partial T}\dot{T} + \frac{\partial\mathcal{N}}{\partial\boldsymbol{C}^{\flat}}:\dot{\boldsymbol{C}}^{\flat}\right) \geq \rho R - \mathrm{Div}\boldsymbol{H} + \frac{1}{T}\left\langle \mathrm{d}T, \boldsymbol{H}\right\rangle\,, \tag{33}$$

where in a local coordinate chart $\{X^A\}$, the 1-form $\mathrm{d}T$ has the representation $\mathrm{d}T = \frac{\partial T}{\partial X^A}dX^A$. The specific free energy function has the form $\Psi = \Psi(X, T, \boldsymbol{C}^{\flat}, \boldsymbol{G})$. The internal energy is defined as the Legendre transform of the free energy with respect to the conjugate variables T and $\mathcal{N}$, i.e., $\mathcal{E} = T\mathcal{N} + \Psi$, and hence, $\mathcal{E} = \mathcal{E}(X, \mathcal{N}, \boldsymbol{C}^{\flat}, \boldsymbol{G})$. Therefore[12]

$$\frac{\partial\mathcal{E}}{\partial\boldsymbol{G}} = T\frac{\partial\mathcal{N}}{\partial\boldsymbol{G}} + \frac{\partial\Psi}{\partial\boldsymbol{G}}\,,\quad \frac{\partial\mathcal{E}}{\partial\boldsymbol{C}^{\flat}} = T\frac{\partial\mathcal{N}}{\partial\boldsymbol{C}^{\flat}} + \frac{\partial\Psi}{\partial\boldsymbol{C}^{\flat}}\,.$$

The localized balance of energy reads [Sadik and Yavari, 2017]

$$\rho\dot{\mathcal{E}} = \boldsymbol{S}:\boldsymbol{D} - \mathrm{Div}\,\boldsymbol{Q} + \rho R + \rho\frac{\partial\mathcal{E}}{\partial\boldsymbol{G}}:\dot{\boldsymbol{G}}\,.$$

This can be rewritten in terms of the specific entropy as

$$\rho\left(\mathcal{N} + \frac{\partial\Psi}{\partial T}\right)\dot{T} + \rho T\frac{\partial\mathcal{N}}{\partial T}\dot{T} + \rho T\frac{\partial\mathcal{N}}{\partial\boldsymbol{C}^{\flat}}:\dot{\boldsymbol{C}}^{\flat} + \left(\rho\frac{\partial\Psi}{\partial\boldsymbol{C}^{\flat}} - \frac{1}{2}\mathbf{S}\right):\dot{\boldsymbol{C}}^{\flat} = \rho R - \mathrm{Div}\,\boldsymbol{H}\,. \tag{34}$$

Substituting (34) into (33) one obtains

$$\rho\left(\mathcal{N} + \frac{\partial\Psi}{\partial T}\right)\dot{T} + \left(\rho\frac{\partial\Psi}{\partial\boldsymbol{C}^{\flat}} - \frac{1}{2}\mathbf{S}\right):\dot{\boldsymbol{C}}^{\flat} + \frac{1}{T}\left\langle \mathrm{d}T, \boldsymbol{H}\right\rangle \leq 0\,.$$

This inequality must hold for all deformations φ and metrics $\boldsymbol{G}$. Therefore[13]

$$\mathcal{N} = -\frac{\partial\Psi}{\partial T},\quad \mathbf{S} = 2\rho\frac{\partial\Psi}{\partial\boldsymbol{C}^{\flat}}\,,\quad \left\langle \mathrm{d}T, \boldsymbol{H}\right\rangle \leq 0\,.$$

[11] AY is grateful to Prof. Marshall Slemrod for a discussion that helped us find and correct this mistake.

[12] These simple relations were written incorrectly in Eq.(62) of Sadik and Yavari [2017].

[13] Note that in addition to the last two relations in Eq.(62), Eq.(66) in [Sadik and Yavari, 2017] is incorrect as well, and the final form of the energy balance in Eq.(69) must be changed to read $\rho T\dot{\mathcal{N}} = \rho R - \mathrm{Div}\,\boldsymbol{H} + \rho T\frac{\partial\mathcal{N}}{\partial\mathbf{G}}:\dot{\mathbf{G}}$. Fortunately, nothing else in [Sadik and Yavari, 2017] was affected by this mistake.